Geobiology

Geobiology (2010), **8**, 197–208 DOI: 10.1111/j.1472-4669.2010.00237.x

Microbial production of isotopically light iron(II) in a modern chemically precipitated sediment and implications for isotopic variations in ancient rocks

G. E. TANGALOS,[1] B. L. BEARD,[1] C. M. JOHNSON,[1] C. N. ALPERS,[2] E. S. SHELOBOLINA,[1] H. XU,[1] H. KONISHI[1] AND E. E. RODEN[1]

[1]*Department of Geoscience and NASA Astrobiology Institute, University of Wisconsin, Madison, WI, USA*
[2]*California Water Science Center, US Geological Survey, Sacramento, CA, USA*

ABSTRACT

The inventories and Fe isotope composition of aqueous Fe(II) and solid-phase Fe compounds were quantified in neutral-pH, chemically precipitated sediments downstream of the Iron Mountain acid mine drainage site in northern California, USA. The sediments contain high concentrations of amorphous Fe(III) oxyhydroxides [$Fe(III)_{am}$] that allow dissimilatory iron reduction (DIR) to predominate over Fe–S interactions in Fe redox transformation, as indicated by the very low abundance of Cr(II)-extractable reduced inorganic sulfur compared with dilute HCl-extractable Fe. δ^{56}Fe values for bulk HCl- and HF-extractable Fe were $\approx$ 0. These near-zero bulk δ^{56}Fe values, together with the very low abundance of dissolved Fe in the overlying water column, suggest that the pyrite Fe source had near-zero δ^{56}Fe values, and that complete oxidation of Fe(II) took place prior to deposition of the Fe(III) oxide-rich sediment. Sediment core analyses and incubation experiments demonstrated the production of millimolar quantities of isotopically light (δ^{56}Fe $\approx$ −1.5 to −0.5‰) aqueous Fe(II) coupled to partial reduction of $Fe(III)_{am}$ by DIR. Trends in the Fe isotope composition of solid-associated Fe(II) and residual $Fe(III)_{am}$ are consistent with experiments with synthetic Fe(III) oxides, and collectively suggest an equilibrium Fe isotope fractionation between aqueous Fe(II) and $Fe(III)_{am}$ of approximately −2‰. These Fe(III) oxide-rich sediments provide a model for early diagenetic processes that are likely to have taken place in Archean and Paleoproterozoic marine sediments that served as precursors for banded iron formations. Our results suggest pathways whereby DIR could have led to the formation of large quantities of low-δ^{56}Fe minerals during BIF genesis.

Received 14 September 2009; accepted 6 March 2010

Corresponding author: Eric E. Roden. Tel.: +1 (608) 890-0724; fax: +1 (608) 262-0693; e-mail: eroden@geology.wisc.edu

INTRODUCTION

Dissimilatory microbial iron reduction (DIR) is a major pathway of organic carbon oxidation in sediments where amorphous Fe(III) oxyhydroxides [$Fe(III)_{am}$] are abundant (Lovley, 1991; Thamdrup, 2000). Dissimilatory iron-reducing microorganisms (DIRMs) use Fe(III) as a terminal electron acceptor in anaerobic respiration, and gain energy by coupling the oxidation of organic compounds or hydrogen to the reduction of Fe(III) oxides (Lovley *et al.*, 2004). DIR has been proposed as a mechanism for the generation of authigenic mineral phases (e.g. siderite and magnetite) in ancient sedimentary environments (Cloud, 1974; Walker, 1984, 1987; Lovley *et al.*, 1987; Nealson & Myers, 1990; Konhauser *et al.*, 2005) that were ultimately preserved in banded iron formations (BIFs). This assertion is consistent with the presence of DIRMs in deeply branching thermophilic and hyperthermophilic prokaryotic lineages (Vargas *et al.*, 1998; Kashefi & Lovley, 2000, 2003; Kashefi *et al.*, 2002).

Analysis of the stable Fe isotope composition of sedimentary rocks provides a potential means for evaluating the contribution of biotic and abiotic Fe redox cycling pathways to sediment diagenesis (Beard *et al.*, 2003; Beard & Johnson, 2004; Johnson *et al.*, 2004). Recent investigations of ancient (Johnson *et al.*, 2003, 2008b; Yamaguchi *et al.*, 2005; Archer & Vance, 2006; Jenkyns *et al.*, 2007) and modern (Bergquist & Boyle, 2006; Severmann *et al.*, 2006, 2008; Staubwasser *et al.*, 2006; Fehr *et al.*, 2008; Homoky *et al.*, 2009; Teutsch *et al.*, 2009) sedimentary environments have explored the relationship between DIR and Fe isotopes. The potential for DIR to produce Fe isotope fractionations observed in natural environments is supported by laboratory studies (Beard *et al.*,

1999, 2003; Crosby *et al.*, 2005, 2007; Johnson *et al.*, 2005; Wu *et al.*, 2009), which indicate that DIR can generate significant quantities of Fe(II) that has negative (isotopically light) δ^{56}Fe values {defined as $10^3 \times [(^{56}Fe/^{54}Fe)_{Sample} - (^{56}Fe/^{54}Fe)_{Std}]/(^{56}Fe/^{54}Fe)_{Std}$, where $(^{56}Fe/^{54}Fe)_{Std}$ is the average Fe isotope composition of igneous rocks (Beard *et al.*, 2003)}, generally between −1‰ and −3‰. These findings are consistent with a key role of DIR in early diagenesis and authigenic mineral formation in Archean and Paleoproterozoic sediments that have preserved large inventories of isotopically light Fe (Johnson *et al.*, 2008a). However, the link between DIR and Fe isotope fractionation has not yet been demonstrated in a natural system where DIR has been shown by microbiological methods to be active in sediment metabolism.

Dissimilatory sulfate reduction (DSR) is the dominant pathway for sediment organic carbon oxidation in modern marine environments (Thamdrup, 2000), and the sulfide produced by this process reacts with sediment Fe to produce Fe-sulfide minerals that have near-zero or slightly positive δ^{56}Fe values (Severmann *et al.*, 2006). Extensive Fe cycling, as recorded, for example, in deposition of BIFs in the Archean and early Proterozoic could not have occurred in the presence of significant sulfide, a conclusion supported by the very low sulfide contents of BIFs (e.g. Klein, 2005). Typical modern marine sediments are thus poor analogs for evaluating the potential influence of DIR on the Fe isotope composition of Archean marine systems.

Temporal variations in the isotopic compositions of marine sedimentary rocks support the idea that DIR and DSR produced distinct isotopic fingerprints at different times during the Archean and Paleoproterozoic eras (Fig. 1). Based on average Fe/S ratios in BIFs (Konhauser *et al.*, 2005) compared with modern marine sediments (Berner, 1982), Fe and S sequestration rates during BIF deposition were likely much higher and lower, respectively, than modern global averages. In particular, deposition of the extensive ~2.5-Ga-old BIFs of the Hamersley Group (Australia) and Transvaal Supergroup (South Africa) occurred during a time of high reactive Fe flux relative to sedimentary sulfide (pyrite) sequestration, and was associated with the largest measured Fe isotope excursion in rocks and minerals known on Earth (Fig. 1A). High rates of reactive Fe flux would have favored DIR over DSR in sediment Fe transformations. Hence, the negative δ^{56}Fe values for magnetite and siderite in BIFs, as well as pyrite in black shales, has been interpreted to reflect mobilization of large quantities of low-δ^{56}Fe aqueous Fe(II) produced by DIR, reflecting a time of maximum expansion of DIR on Earth (Johnson *et al.*, 2008a). Increases in seawater sulfate concentration in the Proterozoic led to an expansion of DSR, which resulted in the onset of low-δ^{34}S sulfide burial (Canfield, 1998; Habicht *et al.*, 2002) (Fig. 1B) and the eventual cessation of BIF deposition (Poulton *et al.*, 2004); an increasing importance of DSR may explain the decrease in the extent of

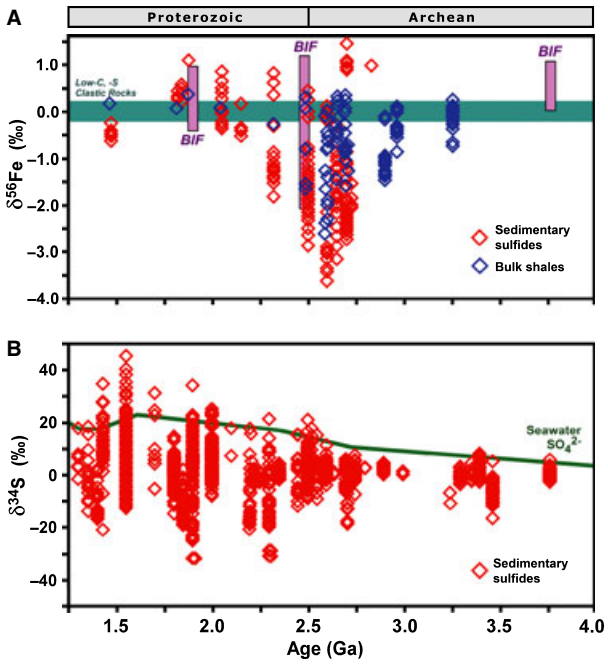

Fig. 1 Temporal variations in Fe and S isotopic compositions of marine sedimentary rocks in the Archean and Paleoproterozoic eras (modified from fig. 7 in Johnson *et al.* (2008a)). (A) The Fe isotope composition of banded iron formations, sedimentary sulfides, and shales has been proposed to record a period of maximum expansion of DIR at the Neoarchean-Paleoproterozoic boundary (~2.5 Ga), reflected in isotopically light magnetite, siderite, and pyrite. (B) The S isotope composition of sedimentary sulfides has been interpreted to record the transition from conditions favoring DIR to expansion of DSR (indicated by the increasing divergence between seawater sulfate and sedimentary sulfide δ^{34}S values). Sulfur and Fe isotope data are from Canfield (2001), Shen *et al.* (2001), Johnson *et al.* (2003, 2008b), Dauphas *et al.* (2004), Rouxel *et al.* (2005, 2006), Yamaguchi *et al.* (2005), Archer & Vance (2006), Frost *et al.* (2007), Severmann *et al.* (2008), Ohmoto *et al.* (2006), Ono *et al.* (2006), Farquhar *et al.* (2007), Whitehouse & Fedo (2007), and Hyslop *et al.* (2008).

Fe isotope fractionation in marine sediments of Paleoproterozoic age (Fig. 1A).

This study reports the results of chemical, isotopic, and microbiological analyses of chemically precipitated sediments in the Spring Creek Arm of the Keswick Reservoir (SCAKR), downstream of the Iron Mountain acid mine drainage (AMD) site in northern CA (Nordstrom & Alpers, 1999). This work provides the first documentation of Fe isotope fractionation in a natural system where DIR activity is demonstrated using microbiological methods. These sediments represent a potential analog to early diagenetic progenitors of banded BIFs in Archean and Paleoproterozoic marine environments. The results demonstrate that DIR can produce very high (millimolar) concentrations of isotopically light (low-δ^{56}Fe) dissolved Fe(II) in Fe-rich, non-sulfidic sediments. This phenomenon provides an explanation for how large quantities of mobile, low-δ^{56}Fe aqueous Fe(II) could have been generated by microbial processes in Neoarchean and Paleoproterozoic marine systems, including early BIF diagenesis.

Site description

Iron Mountain Mine (IMM) is a group of mines within Iron Mountain located in Shasta County, CA (Fig. S1). The commodities Ag, Au, Cu, Fe, Zn, and pyrite (for production of sulfuric acid) were recovered at various times beginning in the early 1860s and terminating with open-pit mining in 1962 (Alpers *et al.*, 2003). AMD effluent from IMM has pH values ranging from the extremely low pH −3.6 within the Richmond Mine portal (Nordstrom & Alpers, 1999) to pH +1.0 to +4.0 in drainage tributaries such as Spring Creek (Edwards *et al.*, 1999; Alpers *et al.*, 2003) (Fig. S1). Total dissolved solid concentrations in the effluent can exceed 900 g L^{-1} (Nordstrom, 2000).

Early AMD mitigation efforts for the Upper Sacramento River watershed affected by IMM effluent involved construction of the Keswick Dam in 1950, which created the Keswick Reservoir and the Spring Creek Debris Dam that serve a barrier to AMD flowing down Spring Creek from IMM (see Fig. S1). Neutral pH water from Whiskeytown Reservoir, part of the Trinity River watershed, flows into Keswick Reservoir through the Spring Creek Power Plant. Mixing of this neutral pH water with Fe-rich AMD from Spring Creek has resulted in the accumulation of three piles (in excess of 260 000 m^3 total bulk volume) of fine-grained, Fe(III) oxide-rich sediment in the SCAKR (Fig. S1). Previous mineralogical characterization of SCAKR sediments via X-ray diffraction (XRD), scanning electron microscopy and Mössbauer spectroscopy identified the presence of ferrihydrite [$Fe(OH)_3$], goethite (α-FeOOH), and mineral structures similar to synthetic schwertmannite [$Fe(III)_8O_8(OH)_6(SO_4)$] (Nordstrom *et al.*, 1999). The sediments have dry weight Fe concentrations ranging from 4% to 47% (mean = 17%), and the pore waters are exceptionally high in aqueous Fe(II) [$Fe(II)_{aq}$], with concentrations ranging up to 36 mM (Nordstrom *et al.*, 1999). The pore waters have pH values of 5.5–6.5, carbonate alkalinities of 0–3 mM, and sulfate concentrations in excess of 10 mM (Nordstrom *et al.*, 1999).

It may be seen counterintuitive that an AMD environment could be an analog to Neoarchean and Paleoproterozoic marine environments, including those involved in BIF formation. It is important to stress, therefore, that the SCAKR sediments formed under circumneutral pH conditions, and that it is their chemical composition that makes them an appropriate model for studying biogeochemical transformations that may have taken place in ancient marine sedimentary environments. Most importantly, the SCAKR sediments contain high concentrations of reactive Fe(III) oxide that (as shown below) result in the predominance of DIR over DSR in early sediment diagenesis, as originally envision by Walker (1984). In addition, the high abundance of reactive Fe(III) permits generation (by DIR) of large quantities of mobile, isotopically light Fe(II). This situation differs dramatically from modern marine sediments, in which large quantities of mobile Fe(II) do not accumulate because reactive Fe becomes incorporated into iron-sulfide minerals (e.g. pyrite). Thus, this setting is envisioned to provide a snapshot of processes that occurred in the sediment pile prior to diagenetic and authigenic formation of magnetite and siderite in BIFs.

MATERIALS AND METHODS

Sample collection and geochemical measurements

Sediments from pile C of the SCAKR site (Nordstrom *et al.*, 1999) were collected by gravity core in 2004 and 2006. Homogenized sediment from different depth intervals were placed in sealed, completely filled glass jars and stored at 4 °C prior to analysis. All samples were handled under anoxic conditions in an anaerobic chamber. Pore fluids were obtained by centrifugation (13 000×*g*, 10 min). Iron in porewater and sediment extracts was measured colorimetrically using *Ferrozine*. Sulfate concentrations were determined by ion chromatography. Solid-phase Fe concentrations were determined via extractions with 0.1 M HCl and/or 0.5 M HCl (see Results and Discussion). Additional extractions were conducted to determine total reactive Fe(III) abundance (0.2 M sodium citrate/0.35 M acetic acid, pH 4.8, plus 50 mg mL^{-1} sodium dithionite) and to recover crystalline Fe phases for Fe isotope analysis (7 M HCl and 29 M HF). Reduced inorganic sulfide was quantified via Cr(II) reduction (Zhabina & Volkov, 1978) and colorimetric sulfide analysis (Cline, 1969). A complete summary of the geochemical data is contained in Tables S1 and S2.

Fe isotope analyses

Iron isotope analyses were performed on pore water Fe, bulk sediment digests, and acid extractions using an MC–ICP–MS (multicollector, inductively coupled plasma mass spectrometer), following established protocols (Beard *et al.*, 2003; Severmann *et al.*, 2006). A summary of the Fe isotope data is provided in SI Table S2.

Sediment incubation experiment

Air-dried sediment from ~150 cm depth in core 06GTIM-A was suspended (28 g L^{-1}) in 10 mM anoxic Pipes buffer (pH 6.7) containing 3 mM sodium acetate to promote Fe(III) reduction. Samples were collected periodically by needle and syringe over a 2-month incubation period and analyzed for aqueous and solid-phase Fe abundance and isotopic composition as described earlier. The geochemical and Fe isotope data from this experiment are included in Tables S1 and S2.

Microbiological analyses

A defined mineral salts medium containing acetate and synthetic $Fe(III)_{am}$ plus vitamins and trace minerals was used

to enumerate DIRMs in roll-tubes with agarized medium as previously described (Shelobolina *et al.*, 2007). The medium was buffered either at pH 6.2 with 10 mM Pipes or 6.8 with 30 mM $NaHCO_3$. The roll-tubes were incubated vertically at 30°C for 8 weeks, after which colonies were enumerated from tubes of appropriate dilution (see Table S3). Individual colonies were transferred to liquid medium containing acetate and synthetic $Fe(III)_{am}$.

Bulk sediment DNA was extracted and purified using the Promega Wizard® Plus SV Minipreps DNA Purification System. 16S rRNA gene sequences were amplified using the universal bacterial forward primer 8F and the reverse primer 1492R. PCR products were cloned using the pGEM®-T vector, and sequenced at the University of Wisconsin-Madison Biotechnology Center. Nearest phylogenetic assignments (see Table S4) were made using the NCBI Basic Local Alignment Search Tool and Taxonomy Browser.

RESULTS AND DISCUSSION

SCAKR sediment properties

Measurements made on three sediment cores collected in 2004 and 2006 showed that SCAKR sediments have a relatively high (mean = 152, range = 26–282) ratio of non-sulfide-associated (citrate/dithionite-extractable) 'reactive Fe' (Canfield, 1989) to reduced inorganic S (see data in Table S1), significantly higher than most modern marine sediments (Raiswell & Canfield, 1998), but similar to oxide- and siderite-facies BIFs from the Kuruman Iron Formation (Klein & Beukes, 1989) and the Dales Gorge member of the Brockman Iron Formation (Ewers & Morris, 1981). Approximately 50–100 mmol L^{-1} of 0.5 M HCl-extractable $Fe(III)_{am}$ is present in SCAKR sediments (Fig. 2A); total (citrate–dithionite extractable) Fe(III) oxide concentrations are 2- to 10-fold higher (see Table S1). Extended extraction of sediment in 0.5 M HCl solubilized ~80% of the total reactive Fe pool (see Fig. S2). These results, along with newly collected XRD and high-resolution transmission electron microscopic analyses (see SI Figs. S3 and S4), verify the previous conclusion (Nordstrom *et al.*, 1999) that most of the Fe(III) oxides are poorly crystalline ferrihydrite and nanocrystalline goethite phases.

The presence of comparable concentrations of 0.5 M HCl-extractable Fe(II) and Fe(III), together with the very high (several mM) porewater $Fe(II)_{aq}$ values (Fig. 2A,B; see Table S1), indicates that DIR is active in SCAKR sediments (Lovley & Phillips, 1987a). The large quantities of Fe(II) in the sediment must originate from internal Fe(III) reduction, given the fact that virtually all of the Fe in the aerobic, circumneutral SCAKR waters is present as colloidal Fe(III) oxide (Alpers *et al.*, 2000). The sediments contain 1.5–4% (dry weight) particulate organic carbon (derived from primary production in the overlying water or inputs of organic matter from the surrounding terrestrial environment), which presumably serves as the source of electron donors for DIR. Although SCAKR sediment pore fluids contain significant concentrations of sulfate (*c.* 4–23 mM; Fig. 2A), DIR dominates Fe transformation as indicated by the absence of acid volatile sulfides and the very low abundance of Cr(II)-extractable reduced inorganic sulfur (pyrite and/or elemental S) compared with dilute HCl-extractable Fe(II) (Fig. 2B). The predominance of DIR over DSR can be attributed to the high concentration of reactive Fe(III) oxides, which allows DIRMs to outcompete dissimilatory sulfate-reducing bacteria for organic electron donors (Lovley & Phillips, 1987b).

An important goal of the current study was to demonstrate the presence and activity of DIRMs through microbiological methods in the same natural samples analyzed for Fe isotope compositions. Fe(III) oxide-containing roll-tube cultures inoculated with serially diluted SCAKR sediment from ~150 cm depth in core 06GTIM-B showed that the abundance of culturable DIRMs ranged from 10^6 to 10^7 cells mL^{-1} (see Table S3), comparable with densities observed in freshwater wetland (Roden & Wetzel, 2002) and other aquatic sediments (Roden & Emerson, 2007) where DIR is active. A 16S rRNA gene sequence clone library from the same sediment (see Table S4) contained sequences closely related (97% similarity) to known DIRMs (*Geobacter* and *Geothrix*). In addition, four different pure culture isolates of *Geothrix fermentans* (97–98% 16S rRNA gene sequence similarity) were obtained by dilution-to-extinction methods (Shelobolina *et al.*, 2007). These results, together with the sediment incubation experiment described below, confirm that DIRMs were active in SCAKR sediments.

Sediment Fe isotope compositions

Aqueous Fe(II) in SCAKR sediment porewater has negative $\delta^{56}Fe$ values compared with bulk HCl-extractable Fe (Fig. 2C). $\delta^{56}Fe$ values for bulk 0.5 M HCl-extractable and total hydrofluoric acid (HF)-extractable Fe fall within the range (shaded field in Fig. 2C) previously defined for terrestrial materials (Beard *et al.*, 2003). The near-zero bulk sediment $\delta^{56}Fe$ values, and the very low abundance of Fe(II) compared with total Fe in the overlying water column (Alpers *et al.*, 2000), suggest that the pyrite Fe source had near-zero $\delta^{56}Fe$ values, essentially equal to the crustal average, and that complete oxidation of Fe(II) took place in the circumneutral pH SCAKR pond prior to deposition of the Fe(III) oxide-rich sediment. This situation differs fundamentally from low-pH AMD environments, in which large variations in the $\delta^{56}Fe$ values of deposited Fe(III) oxides may be attributed to Fe isotope fractionation during partial Fe(II) oxidation and Fe(III) oxide precipitation (Egal *et al.*, 2008).

Partial extraction of pore fluid-free sediment for 1 h with 0.1 M HCl was used to isolate solid-phase Fe(II) [$Fe(II)_s$], which was likely a mixture of sorbed Fe(II) and amorphous

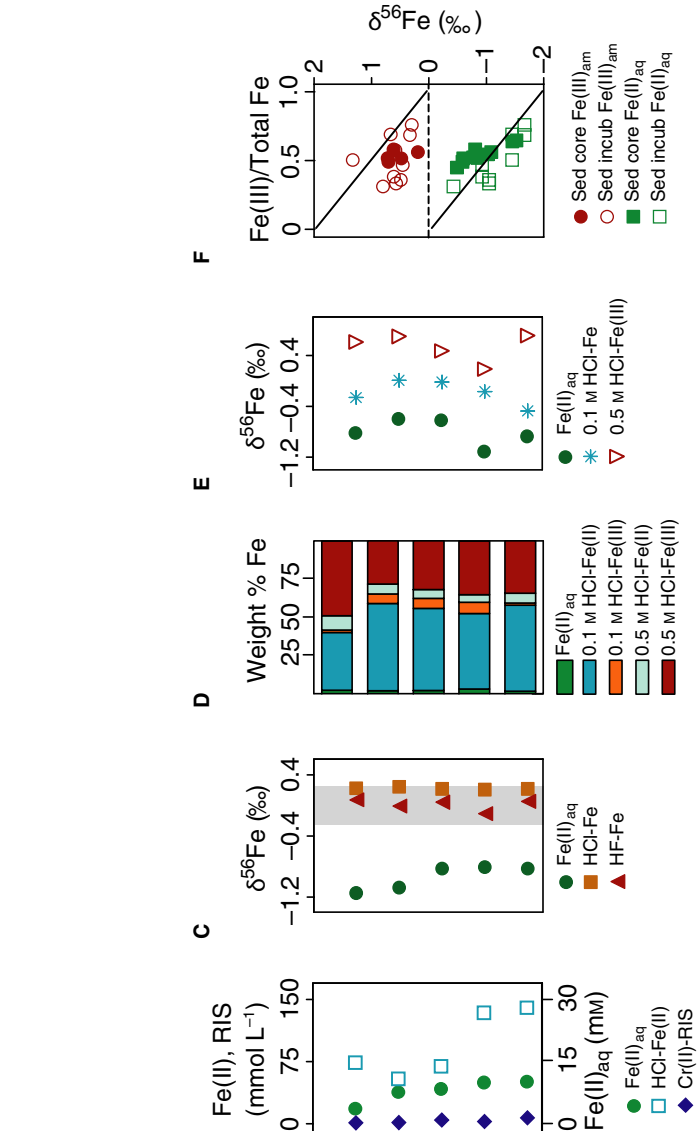

Fig. 2 Geochemical and Fe isotope data for SCAKR sediments. Data are from Tables S1 and S2. (A) Bulk sediment (corrected for porosity) 0.5 M HCl-extractable $Fe(III)_{am}$ and pore fluid SO_4^{2-} concentrations (averages from cores 04CAIM-3, 06GTIM-A, and 06GTIM-B). (B) Pore fluid $Fe(II)_{aq}$ and bulk sediment 0.5 M HCl-extractable Fe(II) (averages from cores 04CAIM-3, 06GTIM-A, and 06GTIM-B) and Cr(II)-extractable reduced inorganic sulfur (RIS) concentrations (data from core 06GTIM-A). (C) $\delta^{56}Fe$ values for pore fluid $Fe(II)_{aq}$, 0.5 M HCl-extractable Fe, and hydrofluoric acid (HF)-extractable Fe (averages from cores 06GTIM-A and 06GTIM-B). Shaded box shows the range of $\delta^{56}Fe$ values for low-C, low-S clastic sedimentary rocks (Beard *et al.*, 2003). (D) Relative abundance (normalized to sediment dry weight) of Fe in different operationally defined pools (data from core 06GTIM-A); 0.1 M HCl and 0.5 M HCl refer to sequential extractions of pore fluid-free sediment; the sum of 0.1 M HCl and 0.5 M HCl-extractable Fe accounted for *c.* 40–60% of total citrate/dithionite-extractable Fe. (E) $\delta^{56}Fe$ values for $Fe(II)_{aq}$, 0.1 M HCl-extractable Fe, and 0.5 M HCl-extractable $Fe(III)_{am}$ (data from core 06GTIM-A); $\delta^{56}Fe$ values for $Fe(III)_{am}$ were computed via isotope mass balance, assuming that the $\delta^{56}Fe$ of Fe(II) recovered in the 0.5 M HCl extract was equal to that of 0.1 M HCl-extractable Fe(II) (see text for details); (F) Relation between $\delta^{56}Fe$ for $Fe(II)_{am}$ (upper panel) and $Fe(II)_{aq}$ (lower panel) and the ratio of Fe(III) to total Fe in 0.5 M HCl extracts of samples of sediment (filled symbols) and laboratory incubations of homogenized sediment (open symbols). Solid lines show a closed-system equilibrium isotope fractionation relation (Criss, 1999) assuming $Fe(II)_{aq}$–$Fe(III)_{am}$ and $Fe(II)_{aq}$–$Fe(II)_s$ fractionations of −2‰ and −0.4‰, respectively, and that ≤10% of total Fe(II) was in the aqueous phase, consistent with data from the sediment cores and incubation experiment.

surface-precipitated Fe(II) hydroxide (Roden & Edmonds, 1997). Fe(II) accounted for >85% of total Fe in the 0.1 M HCl extracts (Fig. 2D; see also Table S2). Subsequent 24-h extraction with 0.5 M HCl recovered $Fe(III)_{am}$ (Fig. 2D) plus some residual $Fe(II)_s$. The Fe isotope composition of the $Fe(III)_{am}$ component in each depth interval was estimated by assuming that Fe(II) in the 0.5 M HCl extract had a $\delta^{56}Fe$ value equal to the Fe in the 0.1 M HCl extract for that depth interval. This approach assumes that partial dissolution of mixed Fe(III)/Fe(II) solids does not cause Fe isotope fractionation, which is consistent with (i) previous studies that have demonstrated that partial dissolution of Fe(III) oxides by dilute HCl does not lead to Fe isotope fractionation (Skulan *et al.*, 2002; Wiederhold *et al.*, 2006); (ii) the consistency of the solid-phase Fe(II)–Fe(III) isotope fractionation observed here and in previous studies (Crosby *et al.*, 2005, 2007); and (iii) the lack of correlation between the 0.1 M and 0.5 M HCl-extractable Fe isotope compositions and the proportion of Fe(II) recovered in the 0.5 M HCl extraction ($r^2 = 0.01$, $n = 16$ including data from the laboratory sediment incubation discussed below). Isotopic mass balance would require such a correlation if Fe isotopes were systematically fractionated during partial HCl dissolution.

The observed trends in Fe isotope fractionations between $Fe(II)_{aq}$, $Fe(II)_s$, and $Fe(III)_{am}$ (Fig. 2E) are similar to those measured in pure culture DIR experiments with crystalline Fe(III) oxides, in which equilibrium Fe isotope exchange between biogenic Fe(II) and 0.5 M HCl-soluble Fe(III) oxide mineral surface atoms has been identified as the mechanism for generation of isotopically light Fe(II) (Crosby *et al.*, 2005, 2007). Isotopic exchange between Fe(II) and bulk $Fe(III)_{am}$ is likely responsible for generation of low-$\delta^{56}Fe$ aqueous Fe(II) in SCAKR sediments, as there was a direct correlation between the $\delta^{56}Fe$ of $Fe(II)_{aq}$ ($\delta^{56}Fe_{Fe(II)aq}$) and the ratio of Fe(III) to total 0.5 M HCl-extractable Fe (Fe_{Tot}) (Fig. 2F), analogous to that between $\delta^{56}Fe_{Fe(II)aq}$ and the ratio of Fe(III) to total Fe in 0.5 M HCl-soluble Fe in crystalline Fe(III) oxide reduction experiments (see fig. 10 in Crosby *et al.*, 2007).

A laboratory experiment was conducted to confirm the ability of indigenous DIRMs to produce the measured Fe isotope compositions in SCAKR sediments. Incubation of oxidized sediment under anaerobic conditions (Fig. 3) produced trends in Fe redox speciation and isotope compositions analogous to those observed *in situ*, i.e. Fe(III) reduction produced mM concentrations of isotopically light $Fe(II)_{aq}$ and rendered the residual $Fe(III)_{am}$ pool slightly (but detectably) heavy relative to the bulk sediment $\delta^{56}Fe$ value of ~0 ‰. Collectively, the data suggest an equilibrium Fe isotope fractionation between $Fe(II)_{aq}$ and $Fe(III)_{am}$ on the order of −2‰, and a smaller but significant fractionation between $Fe(II)_{aq}$ and $Fe(II)_s$ of −0.4‰ (Fig. 2E,F). Both of these values are comparable, though not identical, to results obtained in laboratory DIR experiments with synthetic Fe(III) oxides and pure

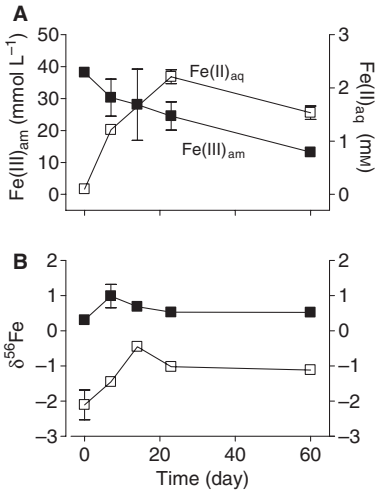

Fig. 3 Changes in Fe redox speciation (A) and Fe isotope composition (B) during laboratory incubation of sediment from ~150 cm depth (see Materials and methods). Data points represent the mean ± range of duplicate sediment suspensions.

DIRMs cultures (Crosby *et al.*, 2005, 2007; Johnson *et al.*, 2005; Wu *et al.*, 2009). The fact that the observed $Fe(II)_{aq}$–$Fe(III)_{am}$ fractionation is less negative (by *c.* 1‰) than that documented for $Fe(II)_{aq}$ and $Fe(III)_{aq}$ in solution (Welch *et al.*, 2003), and for $Fe(II)_{aq}$ and surface Fe(III) atoms on hematite (Crosby *et al.*, 2005, 2007), may reflect the smaller $Fe(II)_{aq}$–goethite Fe isotope fractionation factor relative to $Fe(II)_{aq}$–hematite (Beard *et al.*, 2009), as well as potential differences in Fe(II) and Fe(III) bonding in complex DIR systems (Wu *et al.*, 2009).

The $\delta^{56}Fe_{Fe(II)aq}$ values in SCAKR sediments (−0.8‰ to −1.2‰) are less negative than those documented for the surficial Fe(III)-reducing zone of modern marine sediments (−1.3‰ to −3‰) (Bergquist & Boyle, 2006; Severmann *et al.*, 2006; Homoky *et al.*, 2009), or stratified water columns (Teutsch *et al.*, 2009). This contrast is probably related to differences in Fe redox cycling and redistribution, processes that concentrate on isotopically light Fe (both aqueous and solid-phase) near the aerobic–anaerobic interface (Staubwasser *et al.*, 2006). In modern marine sediments, for example, near-surface oxidation of low-$\delta^{56}Fe$ aqueous Fe(II) produces low-$\delta^{56}Fe$ reactive Fe(III) oxides, which, when partially reduced by DIRMs, may produce $Fe(II)_{aq}$ that has very low $\delta^{56}Fe$ values (Severmann *et al.*, 2006; Homoky *et al.*, 2009). The extremely rapid and voluminous deposition of $Fe(III)_{am}$ in the SCAKR probably limited the extent of Fe redox cycling and redistribution at this site. Likewise, the high depositional rates and slightly subneutral pH (6.2–6.5) has prevented conversion of Fe(II) to commonly observed end products of microbial $Fe(III)_{am}$ reduction such as magnetite and siderite (Walker, 1984), neither of which were detected by XRD nor transmission electron microscopic analysis (see Figs. S3 and S4).

Implications for BIF genesis in the Archean and Paleoproterozoic

Most models for BIF formation involve two stages: an initial water column stage during which hydrothermally sourced $Fe(II)_{aq}$ is oxidized in the photic zone of the oceans, resulting in deposition of Fe(III) oxides to the seafloor; followed by a sediment diagenetic stage where $Fe(II)_{aq}$ reacts with deposited Fe(III) oxides to produce magnetite [or mixed Fe(II)–Fe(III) hydroxide magnetite precursor phases], or with carbonate or dissolved silica to produce siderite or Fe(II)-bearing silicate phases (e.g. Klein, 2005; Beukes & Gutzmer, 2008). Partial oxidation of hydrothermal Fe(II) will produce positive δ^{56}Fe values for Fe(III) oxide precipitates, whereas complete oxidation will produce δ^{56}Fe values in the precipitates that match those of the source Fe(II) (e.g. Bullen *et al.*, 2001; Rouxel *et al.*, 2003, 2008; Severmann *et al.*, 2004). Positive δ^{56}Fe values for oxide minerals in BIFs are generally accepted to reflect partial oxidation of aqueous Fe(II) (Johnson *et al.*, 2003; Dauphas *et al.*, 2004; Rouxel *et al.*, 2005; Dauphas *et al.*, 2007a,b; Frost *et al.*, 2007; Whitehouse & Fedo, 2007; Johnson *et al.*, 2008b; Valaas-Hyslop *et al.*, 2008; Planavsky *et al.*, 2009; Steinhoefel *et al.*, 2009). Extensive oxidation of $Fe(II)_{aq}$ produces low-δ^{56}Fe values in the remaining Fe(II) (Bullen *et al.*, 2001; Croal *et al.*, 2003; Balci *et al.*, 2006; Rouxel *et al.*, 2008). Coupling of biotic and/or abiotic Fe(II) oxidation to deposition of positive δ^{56}Fe Fe(III) oxides in continental margin sediments could have shifted $Fe(II)_{aq}$ in deep anoxic basin waters to negative δ^{56}Fe values, leading to the eventual burial of low-δ^{56}Fe pyrite (Rouxel *et al.*, 2005). However, this process cannot account for the formation of low-δ^{56}Fe magnetite and siderite in Fe-rich sediments such as BIFs, because the amount of low-δ^{56}Fe $Fe(II)_{aq}$ generated during extensive $Fe(II)_{aq}$ oxidation is relatively small (see fig. 1 in Johnson *et al.*, 2008a). As recently suggested by Steinhoefel *et al.* (2009), strata within BIF deposits that form during input of relatively low amounts of Fe are likely to be dominated by chert as opposed to Fe minerals. The key implication of this is that the production of relatively small amounts of low-δ^{56}Fe $Fe(II)_{aq}$ during near-complete oxidation of Fe(II) in the water column is not likely to have led to the formation of Fe-rich, low-δ^{56}Fe rocks. An alternative process for producing large quantities of low-δ^{56}Fe aqueous Fe(II) is required.

Fe(III) oxide deposits associated with modern hydrothermal vent systems (e.g. Bonatti & Joensuu, 1966; Karl *et al.*, 1988; Rouxel *et al.*, 2003; Severmann *et al.*, 2004) may be considered as analogs to the first stage of BIF formation. They are not, however, complete BIF analogs because they do not account for the significant inventory of Fe(II) in BIF minerals such as magnetite and siderite. In addition, such deposits are not connected to carbon-cycling processes in a manner analogous to widely accepted models for BIF genesis, in which photosynthesis (oxygenic or anoxygenic)-driven Fe(II) oxidation led to codeposition of Fe(III) oxides and organic matter that served as substrates for DIR (Walker, 1984, 1987; Kappler *et al.*, 2005; Konhauser *et al.*, 2005). DIR provides an explanation for the large inventory of Fe(II) in BIFs, as well as the highly negative δ^{13}C values for BIF carbonates that have been interpreted to record oxidation of photosynthetically derived organic matter (Becker & Clayton, 1972; Walker, 1984; Baur *et al.*, 1985; Beukes & Gutzmer, 2008; Fischer *et al.*, 2009).

The initial end product of DIR is aqueous Fe(II), which is likely to have been present in relatively high concentrations in Fe(III)-reducing BIF precursor sediments. Because the aqueous Fe(II) component is not preserved in ancient rocks such as BIFs, modern systems are needed to understand the potential mechanisms that can produce Fe(II)-bearing BIF minerals, in particular those with low δ^{56}Fe values. Studies in modern continental margin sediments have provided important information on how DIR could have caused Fe isotope fractionation during early diagenesis in ancient marine sediments (Severmann *et al.*, 2006). However, Fe transformation in these sediments is influenced by interactions with sulfur to a much greater extent than was the case in S-poor BIF precursor sediments.

The SCAKR site provides insight into the role of $Fe(II)_{aq}$ in BIF genesis that cannot be determined from the rock record because aqueous components are lost upon lithification. The site is an analog to relatively shallow-water shelf environments in which near-complete oxidation of incoming, hydrothermally sourced Fe(II) [resulting in the deposition of near-zero δ^{56}Fe Fe(III) oxides] may have taken place in conjunction with oxygenic or anoxygenic photosynthesis, leading to codeposition of Fe(III) oxides and modest amounts of labile organic matter whose oxidation fueled DIR activity. High concentrations of $Fe(III)_{am}$ would have suppressed DSR and allow DIR to dominate sediment Fe diagenesis in a manner analogous to that inferred for BIFs (Walker, 1984). In essence, this scenario corresponds to that envisioned by Severmann *et al.* (2008) based on solid-phase Fe isotope analyses on Black Sea sediments, in which DIR in continental shelf sediments is responsible for the mobilization of isotopically light Fe that is eventually captured in pyrite in deep euxinic basin shale deposits. This benthic Fe shuttle model provides a mechanism for producing bulk changes in δ^{56}Fe values of marine sedimentary rocks. In addition, as noted in Johnson *et al.* (2008a), DIR driven by sustained burial flux of Fe(III) oxide and organic carbon can create a continual source of low-δ^{56}Fe Fe(II), which by diffusion or other transport processes could result in large-scale Fe isotope redistribution across sediment layers (Ewers, 1983). The work presented here extends this model by documenting production by DIR of very high concentrations of isotopically light $Fe(II)_{aq}$ in pore fluids, analogous to $Fe(II)_{aq}$-rich pore fluids in modern marine sediments that have been inferred, but not proven, to have been produced by DIR (Bergquist & Boyle, 2006; Severmann *et al.*, 2006; Rouxel *et al.*, 2008).

We stress that the SCAKR sediment is envisioned as an analog to the earliest stages of near-surface BIF diagenesis, where aqueous Fe(II) interacted with ferric oxide/hydroxides or precipitated Fe(II)-bearing minerals from solution. Later diagenetic and authigenic mineral formation pathways are required to produce the minerals observed in BIFs, including dewatering/compaction and modest heating, ultimately leading to the formation of consolidated magnetite- and/or siderite-rich layered deposits (Klein, 2005). This is consistent with most models for BIF formation, where poorly crystalline silica, aqueous Fe(II), and Fe(III) oxide in fluid-rich gels are envisioned to be precursors to chert, magnetite, siderite, and Fe(II) silicates (e.g. Klein, 2005; Beukes & Gutzmer, 2008).

Figure 4 presents conceptual depictions of how the production of isotopically light Fe(II) by DIR in such sediments could eventually lead to the formation of major BIF minerals such as magnetite and siderite, as well as sedimentary pyrite, which may have negative δ^{56}Fe values in the range of those observed in BIFs and black shales (see Fig. 1B). This model assumes implicitly that the Fe(III) oxides undergoing reduction were first produced by near-complete oxidation of hydrothermally derived Fe(II) (in the water column) that had a δ^{56}Fe value close to zero. In all cases, partial reduction of $Fe(III)_{am}$ is the mechanism responsible for mobilization of low-δ^{56}Fe aqueous Fe(II), which is subsequently transported away from the locus of DIR and eventually incorporated into Fe(II)-bearing minerals. It must be emphasized that the processes depicted in Fig. 4 are not meant to imply periodicity or to explain the formation of different types of banding structures present in BIFs, but rather simply to illustrate how isotopically light Fe(II) may be mobilized by DIR and later incorporated into such layered deposits that reflect authigenic mineral formation prior to lithification.

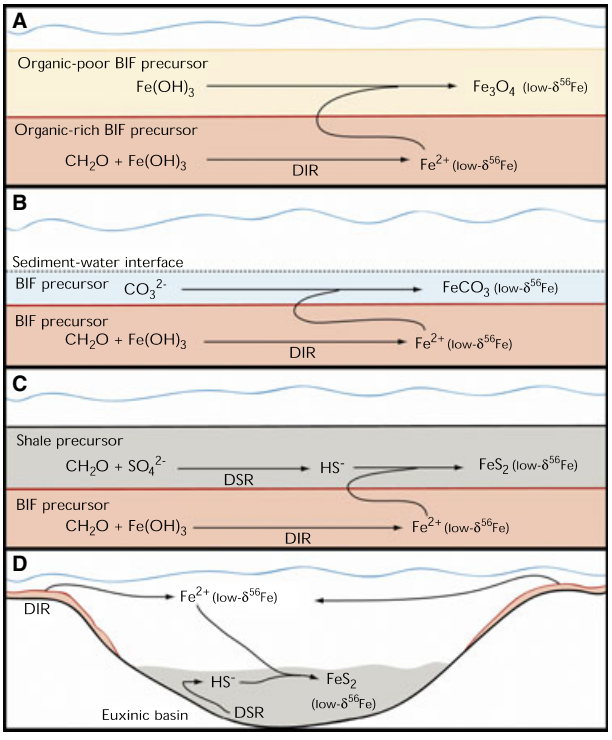

Fig. 4 Conceptual models for how production and transport (via diffusion/dispersion or advection) of low-δ^{56}Fe aqueous Fe(II) by DIR in BIF precursor sediments could have led to generation of low-δ^{56}Fe magnetite, siderite, and pyrite in Archean and Paleoproterozoic rocks. Note that the Fe(III) oxides undergoing reduction are presumed to have originated from near-complete oxidation of hydrothermally derived Fe(II) in the water column. (A) Transport from organic-rich sediments (active DIR) to organic-poor sediments (little or no DIR) and reaction with $Fe(III)_{am}$ to form isotopically light magnetite via solid-state conversion (Hansel *et al.*, 2003). (B) Transport to the sediment–water interface followed by reaction with dissolved carbonate to form a layer of low-δ^{56}Fe siderite. (C) Transport into an organic-rich siliciclastic layer supporting DSR and reaction with sulfide to produce low-δ^{56}Fe pyrite (Archer & Vance, 2006; Severmann *et al.*, 2006). (D) Release from continental margin sediments, followed by transport into an adjacent deep euxinic basin and reaction with sulfide to form low-δ^{56}Fe pyrite (Severmann *et al.*, 2008).

A key question that arises from the above conceptual model is the fate of the isotopically heavy Fe(III) oxide left behind after mobilization of low-δ^{56}Fe aqueous Fe(II). Recent work on siderite-bearing BIF strata from the Kuruman Iron Formation and underlying BIF and platform Ca–Mg carbonates of the Gamohaan Formation in South Africa (Heimann *et al.*, 2010) has documented the presence, in some strata, of low-δ^{13}C, high-δ^{56}Fe siderite that are likely to have formed by near-complete reduction by DIR of high-δ^{56}Fe Fe(III) oxides that were left over from prior partial Fe(III) reduction by DIR. An interesting related observation is the common occurrence of hematite inclusions in the high-δ^{56}Fe siderite-bearing strata, which may represent small amounts of residual crystalline Fe(III) oxide that remained resistant to microbial reduction. The combined Fe, C, and O isotope data from the Heimann *et al.*'s (2010) study are consistent with the conceptual model in Fig. 4, in which differential Fe mobilization by DIR, prior to lithification, plays a key role in determining the range of δ^{56}Fe values of BIF mineral phases. On a basin-wide scale, Czaja *et al.* (2010) note that low-δ^{56}Fe values for black shales in the central part of the 2.7-Ga Hamersley basin were balanced by slightly positive values for coeval sediments on the margin of the basin, consistent with the benthic Fe shuttle model of Severmann *et al.* (2008). These observations emphasize the key issue of basin-scale isotope mass balance in interpreting the Fe isotope composition of ancient rocks. All of these results support previous (Walker, 1984) and ongoing (Vargas *et al.*, 1998; Johnson *et al.*, 2008a) inferences regarding the prominence of DIR in sediment biogeochemical cycling on the early Earth.

ACKNOWLEDGEMENTS

This research was funded by the NASA Astrobiology Institute (University of California-Berkeley and University of Wisconsin-Madison nodes) and the National Science Foundation

(Biogeosciences Program Award 0525417). Logistical support for field sampling was provided by the US Geological Survey in cooperation with the US Environmental Protection Agency. We thank Kurt Konhauser and three anonymous reviewers whose thoughtful criticism substantially improved the manuscript.

REFERENCES

Alpers CN, Antweiler RC, Taylor HE, Dileanis PD, Domagalski JL (2000) *Metals Transport in the Sacramento River, California, 1996–1997, Volume 2: Interpretation of Metal Loads*. US Geological Survey Water-Resources Investigation Report, Sacramento, CA, pp. 99–4286.

Alpers CN, Nordstrom DK, Spitzley J (2003) Extreme acid mine drainage from a pyritic massive sulfide deposit: the Iron Mountain end member. In *Environmental Aspects of Mine-Wastes* (eds Jambor JL, Blowes DW, Ritchie AIM). Mineralogical Association of Canada, Ottawa, pp. 407–430.

Archer C, Vance D (2006) Couple Fe and S isotope evidence for Archean microbial Fe(III) and sulfate reduction. *Geology* **34**, 153–156.

Balci N, Bullen TD, Witte- Lien K, Shanks WC, Motelica M, Mandernack KW (2006) Iron isotope fractionation during microbially stimulated Fe(II) oxidation and Fe(III) precipitation. *Geochimica et Cosmochimica Acta* **70**, 622–639.

Baur ME, Hayes JM, Studley SA, Walter MR (1985) Millimeter-scale variations of stable isotope abundances in carbonates from banded iron-formations in the Hamersley Group of Western-Australia. *Economic Geology* **80**, 270–282.

Beard BL, Johnson CM (2004) Fe isotope variations in the modern and ancient earth and other planetary bodies. In *Geochemistry of Non-Traditional Stable Isotopes, Reviews in Mineralogy and Geochemistry 55* (eds Johnson CM, Beard BL, Albarede F). Mineralogical Society of America, Washington, DC, pp. 319–357.

Beard BL, Johnson CM, Cox L, Sun H, Nealson KH, Aguilar C (1999) Iron isotope biosignatures. *Science* **285**, 1889–1891.

Beard BL, Johnson CM, Skulan JL, Nealson KH, Cox L, Sun H (2003) Application of Fe isotopes to tracing the geochemical and biological cycling of Fe. *Chemical Geology* **195**, 85–117.

Beard BL, Handler R, Johnson CM, Scherer M (2009) Experimental determination of the Fe isotope fractionation between Fe(II) and goethite. *Geochimica et Cosmochimica Acta* **73**, A99.

Becker RH, Clayton RN (1972) Carbon isotopic evidence for the origin of a banded iron-formation in Western Australia. *Geochimica et Cosmochimica Acta* **36**, 577–595.

Bergquist BA, Boyle EA (2006) Iron isotopes in the Amazon River system: weathering and transport signatures. *Earth and Planetary Science Letters* **248**, 54–68.

Berner RA (1982) Burial of organic carbon and pyrite sulfur in the modern ocean: its geochemical and environmental significance. *American Journal of Science* **282**, 451–473.

Beukes NJ, Gutzmer J (2008) Origin and paleoenvironmental significance of major iron formations at the Archean-Paleoproterozoic boundary. *Reviews in Economic Geology Series* **15**, 5–47.

Bonatti E, Joensuu O (1966) Deep-sea iron deposit from south pacific. *Science* **154**, 643.

Bullen TD, White AF, Childs CW, Vivit DV, Schulz MS (2001) Demonstration of significant abiotic iron isotope fractionation in nature. *Geology* **29**, 699–702.

Canfield DE (1989) Reactive iron in marine sediments. *Geochimica et Cosmochimica Acta* **53**, 619–632.

Canfield DE (1998) A new model for proterozoic ocean chemistry. *Nature* **396**, 450–661.

Canfield DE (2001) Biogeochemistry of sulfur isotopes. In *Stable Isotope Geochemistry, Reviews in Mineralogy and Geochemistry 43* (eds Valley JW, Cole DR). Mineralogical Society of America, Washington, DC, pp. 607–636.

Cline JD (1969) Spectrophotometric determination of hydrogen sulfide in natural waters. *Limnology and Oceanography* **14**, 454–458.

Cloud P (1974) Evolution of ecosystems. *American Scientist* **62**, 54–66.

Criss RE (1999) *Principles of Stable Isotope Distribution*. Oxford University Press, New York.

Croal LR, Johnson CM, Beard BL, Newman DK (2003) Iron isotope fractionation by anoxygenic Fe(II)-phototrophic bacteria. *Geochimica et Cosmochimica Acta* **68**, 1227–1242.

Crosby HA, Johnson CM, Roden EE, Beard BL (2005) Fe(II)-Fe(III) electron/atom exchange as a mechanism for Fe isotope fractionation during dissimilatory iron oxide reduction. *Environmental Science and Technology* **39**, 6698–6704.

Crosby HA, Johnson CM, Beard BL, Roden EE (2007) The mechanisms of iron isotope fractionation produced during dissimilatory Fe(III) reduction by *Shewanella putrefaciens* and *Geobacter sulfurreducens*. *Geobiology* **5**, 169–189.

Czaja AD, Johnson CM, Beard BL, Eigenbrode JL, Freeman KH, Yamaguch KE (2010) Iron and carbon isotope evidence for ecosystem and environmental diversity in the ~2.7 to 2.5 Ga Hamersley Province, Western Australia. *Earth and Planetary Science Letters* **292**, 170–180.

Dauphas N, van Zuilen M, Wadhwa M, Davis AM, Marty B, Janney PE (2004) Clues from Fe isotope variations on the origin of early Archean BIFs from Greenland. *Science* **306**, 2077–2080.

Dauphas N, Cates NL, Mojzsis SJ, Busigny V (2007a) Identification of chemical sedimentary protoliths using iron isotopes in the >3750 Ma Nuvvuagittuq supracrustal belt, Canada. *Earth and Planetary Science Letters* **254**, 358–376.

Dauphas N, Van Zuilen M, Busigny V, Lepland A, Wadhwa M, Janney PE (2007b) Iron isotope, major and trace element characterization of early Archean supracrustal rocks from SW Greenland: protolith identification and metamorphic overprint. *Geochimica et Cosmochimica Acta* **71**, 4745–4770.

Edwards KJ, Gihring TM, Banfield JF (1999) Seasonal variations in microbial populations and environmental conditions in an extreme acid mine drainage environment. *Applied and Environmental Microbiology* **65**, 3627–3632.

Egal M, Elbaz-Poulichet F, Casiot C, Motelica-Heino M, Negrel P, Bruneel O, Sarmiento AM, Nieto JM (2008) Iron isotopes in acid mine waters and iron-rich solids from the Tinto-Odiel Basin (Iberian Pyrite Belt, Southwest Spain). *Chemical Geology* **253**, 162–171.

Ewers WE (1983) Chemical factors in the deposition and diagenesis of banded iron-formations. In *Iron-Formation: Facts and Problems* (eds Trendall AF, Morris RC). Elsevier, Amsterdam, pp. 491–512.

Ewers WE, Morris RC (1981) Studies of the Dales-Gorge-member of the Brockman-Iron-Formation, Western Australia. *Economic Geology* **76**, 1929–1953.

Farquhar J, Peters M, Johnston DT, Strauss H, Masterson A, Wiechert U, Kaufman AJ (2007) Isotopic evidence for Mesoarchaean anoxia and changing atmospheric sulphur chemistry. *Nature* **449**, 706–709.

Fehr MA, Andersson PS, Halenius U, Morth CM (2008) Iron isotope variations in Holocene sediments of the Gotland Deep, Baltic Sea. *Geochimica et Cosmochimica Acta* **72**, 807–826.

Fischer WW, Schroeder S, Lacassie JP, Beukes NJ, Goldberg T, Strauss H *et al.* (2009) Isotopic constraints on the Late Archean carbon cycle from the Transvaal Supergroup along the western margin of the Kaapvaal Craton, South Africa. *Precambrian Research* **169**, 15–27.

Frost CD, von Blanckenburg F, Schoenberg R, Frost BR, Swapp SM (2007) Preservation of Fe isotope heterogeneities during diagenesis and metamorphism of banded iron formation. *Contributions to Mineralogy and Petrology* **153**, 211–235.

Habicht KS, Gade M, Thamdrup B, Berg P, Canfield DE (2002) Calibration of sulfate levels in the Archean Ocean. *Science* **298**, 2372–2374.

Hansel CM, Benner SG, Neiss J, Dohnalkova A, Kukkadapu RK, Fendorf S (2003) Secondary mineralization pathways induced by dissimilatory iron reduction of ferrihydrite under advective flow. *Geochimica et Cosmochimica Acta* **67**, 2977–2992.

Heimann A, Johnson CM, Beard BL, Valley JW, Roden EE, Spicuzza MJ, Beukes NJ (2010) Fe, C, and O isotope compositions of banded iron formation carbonates demonstrate a major role for dissimilatory iron reduction in ~2.5 Ga marine environments. *Earth and Planetary Science Letters*. doi:10.1016/j.epsl.2010.02.015.

Homoky WB, Severmann S, Mills RA, Statham PJ, Fones GR (2009) Pore-fluid Fe isotopes reflect the extent of benthic Fe redox recycling: evidence from continental shelf and deep-sea sediments. *Geology* **37**, 751–754.

Hyslop EV, Valley JW, Johnson CM, Beard BL (2008) The effects of metamorphism on O and Fe isotope compositions in the Biwabik Iron Formation, northern Minnesota. *Contributions to Mineralogy and Petrology* **155**, 313–328.

Jenkyns HC, Matthews A, Tsikos H, Erel Y (2007) Nitrate reduction, sulfate reduction, and sedimentary iron isotope evolution during the Cenomanian-Turonian oceanic anoxic event. *Paleoceanography* **22**, PA3208.

Johnson CM, Beard BL, Beukes NJ, Klein C, O'Leary JM (2003) Ancient geochemical cycling in the Earth as inferred from Fe isotope studies of banded iron formations from the Transvaal Craton. *Contributions to Mineralogy and Petrology* **144**, 523–547.

Johnson CM, Beard BL, Roden EE, Newman DK, Nealson KH (2004) Isotopic constraints on biogeochemical cycling of Fe. In *Geochemistry of Non-Traditional Stable Isotopes, Reviews in Mineralogy and Geochemistry 55* (eds Johnson CM, Beard BL, Albarède F). Mineralogical Society of America, Washington, DC, pp. 359–408.

Johnson CM, Roden EE, Welch SA, Beard BL (2005) Experimental constraints on Fe isotope fractionation during magnetite and Fe carbonate formation coupled to dissimilatory hydrous ferric oxide reduction. *Geochimica et Cosmochimica Acta* **69**, 963–993.

Johnson CM, Beard BL, Roden EE (2008a) The iron isotope fingerprints of redox and biogeochemical cycling in the modern and ancient Earth. *Annual Review of Earth and Planetary Sciences* **36**, 457–493.

Johnson CM, Beard BL, Klein C, Beukes NJ, Roden EE (2008b) Iron isotopes constrain biologic and abiologic processes in banded iron formation genesis. *Geochimica et Cosmochimica Acta* **72**, 151–169.

Kappler A, Pasquero C, Konhauser KO, Newman DK (2005) Deposition of banded iron formations by anoxygenic phototrophic Fe(II)-oxidizing bacteria. *Geology* **33**, 865–868.

Karl DM, McMurtry GM, Malahoff A, Garcia MO (1988) Loihi seamount, Hawaii: a mid-plate volcano with a distinctive hydrothermal system. *Nature* **335**, 532–535.

Kashefi K, Lovley D (2000) Reduction of Fe(III), Mn(IV) and Toxic Metals at 100°C by *Pyrobaculum islandicum*. *Applied and Environmental Microbiology* **66**, 1050–1056.

Kashefi K, Lovley DR (2003) Extending the upper temperature limit for life. *Science* **301**, 934.

Kashefi K, Tor JM, Holmes DE, Van Praagh CVG, Reysenbach AL, Lovley DR (2002) *Geoglobus ahangari* gen. nov., sp nov., a novel hyperthermophilic archaeon capable of oxidizing organic acids and growing autotrophically on hydrogen with Fe(III) serving as the sole electron acceptor. *International Journal of Systematic and Evolutionary Microbiology* **52**, 719–728.

Klein C (2005) Some Precambrian banded iron-formations (BIFs) from around the world: their age, geologic setting, mineralogy, metamorphism, geochemistry, and origin. *American Mineralogist* **90**, 1473–1499.

Klein C, Beukes NJ (1989) Geochemistry and sedimentology of a facies transition from limestone to iron-formation deposition in the Early Proterozoic Transvaal Supergroup, South-Africa. *Economic Geology* **84**, 1733–1774.

Konhauser KO, Newman DK, Kappler A (2005) The potential significance of microbial Fe(III) reduction during deposition of Precambrian banded iron formations. *Geobiology* **3**, 167–177.

Lovley DR (1991) Dissimilatory Fe(III) and Mn(IV) reduction. *Microbiological Reviews* **55**, 259–287.

Lovley DR, Phillips EJP (1987a) Rapid assay for microbially reducible ferric iron in aquatic sediments. *Applied and Environmental Microbiology* **53**, 1536–1540.

Lovley DR, Phillips EJP (1987b) Competitive mechanisms for inhibition of sulfate reduction and methane production in the zone of ferric iron reduction in sediments. *Applied and Environmental Microbiology* **53**, 2636–2641.

Lovley DR, Stolz JF, Nord GL, Phillips EJP (1987) Anaerobic production of magnetite by a dissimilatory iron-reducing microorganism. *Nature* **330**, 252–254.

Lovley DR, Holmes DE, Nevin KP (2004) Dissimilatory Fe(III) and Mn(IV) reduction. *Advances in Microbial Physiology* **49**, 219–286.

Nealson KH, Myers CR (1990) Iron reduction by bacteria: a potential role in the genesis of banded iron formations. *American Journal of Science* **290**, 35–45.

Nordstrom DK (2000) Advances in the hydrogeochemistry and microbiology of acid mine waters. *International Geology Review* **42**, 499–515.

Nordstrom DK, Alpers CN (1999) Negative pH, efflorescent mineralogy, and consequences for environmental restoration at the Iron Mountain Superfund Site, California. *Proceedings of the National Academy of Sciences of the USA* **96**, 3455–3462.

Nordstrom DK, Alpers CN, Coston JA, Taylor HE, McCleskey RB, Ball JW *et al.* (1999) Geochemistry, toxicity, and sorption properties of contaminated sediments and pore waters in two reservoirs receiving acid mine drainage from Iron Mountain, California. In *Proceedings of the US Geological Survey Toxic Substances Hydrology Program* (eds Morganwalp DW, Buxton HT). US Geological Survey Water-Resources Investigation Report, Sacramento, CA, pp. 289–296.

Ohmoto H, Watanabe Y, Ikemi H, Poulson SR, Taylor BE (2006) Sulphur isotope evidence for an oxic Archaean atmosphere. *Nature* **442**, 908–911.

Ono S, Beukes NJ, Rumble D, Fogel ML (2006) Early evolution of atmospheric oxygen from multiple-sulfur and carbon isotope records of the 2.9 Ga Mozaan Group of the Pongola Supergroup, Southern Africa. *South African Journal of Geology* **109**, 97–108.

Planavsky N, Rouxel O, Bekker A, Shapiro R, Fralick P, Knudsen A (2009) Iron-oxidizing microbial ecosystems thrived in late Paleoproterozoic redox-stratified oceans. *Earth and Planetary Science Letters* **286**, 230–242.

Poulton SW, Fralick PW, Canfield DE (2004) The transition to a sulphidic ocean similar to 1.84 billion years ago. *Nature* **431**, 173–177.
Raiswell R, Canfield DE (1998) Sources of iron for pyrite formation in marine sediments. *American Journal of Science* **298**, 219–245.
Roden EE, Edmonds JW (1997) Phosphate mobilization in iron-rich anaerobic sediments: microbial Fe(III) oxide reduction versus iron-sulfide formation. *Archiv für Hydrobiologie* **139**, 347–378.
Roden EE, Emerson D (2007) Microbial metal cycling in aquatic environments. In *Manual of Environmental Microbiology*, 3rd edn (eds Hurst CJ, Lipson D, Crawford R, Garland J, Mills A, Stezenbach LD). American Society for Microbiology, Washington, DC, pp. 540–562.
Roden EE, Wetzel RG (2002) Kinetics of microbial Fe(III) oxide reduction in freshwater wetland sediments. *Limnology and Oceanography* **47**, 198–211.
Rouxel O, Dobbek N, Ludden J, Fouquet Y (2003) Iron isotope fractionation during oceanic crust alteration. *Chemical Geology* **202**, 155–182.
Rouxel O, Bekker A, Edwards K (2005) Iron isotope constraints on the Archean and Paleoproterozoic ocean redox state. *Science* **307**, 1088–1091.
Rouxel OJ, Bekker A, Edward KJ (2006) Response to comment on "Iron isotope constraints on the archean and paleoproterozoic ocean redox state". *Science* **311**, 177.
Rouxel O, Sholkovitz E, Charette M, Edwards KJ (2008) Iron isotope fractionation in subterranean estuaries. *Geochimica et Cosmochimica Acta* **72**, 3413–3430.
Severmann S, Johnson CM, Beard BL, German CR, Edmonds HN, Chiba H, Green DRH (2004) The effect of plume processes on the Fe isotope composition of hydrothermally derived Fe in the deep ocean as inferred from the Rainbow vent site, Mid-Atlantic Ridge, 36 degrees 14' N. *Earth and Planetary Science Letters* **225**, 63–76.
Severmann S, Johnson CM, Beard BL, McManus J (2006) The effect of early diagenesis on the Fe isotope compositions of porewaters and authigenic minerals in continental margin sediments. *Geochimica et Cosmochimica Acta* **70**, 2006–2022.
Severmann S, Lyons TW, Anbar A, McManus J, Gordon G (2008) Modern iron isotope perspective on the benthic iron shuttle and the redox evolution of ancient oceans. *Geology* **36**, 487–490.
Shelobolina ES, Nevin KP, Blakeney-Hayward JD, Johnsen CV, Plaia TW, Krader P *et al.* (2007) *Geobacter pickeringii* sp. nov., *Geobacter argillaceus* sp. nov. and *Pelosinus fermentans* gen. nov., sp. nov., isolated from subsurface kaolin lenses. *International Journal of Systematic and Evolutionary Microbiology* **56**, 126–135.
Shen YA, Buick R, Canfield DE (2001) Isotopic evidence for microbial sulphate reduction in the early Archaean era. *Nature* **410**, 77–81.
Skulan JL, Beard BL, Johnson CM (2002) Kinetic and equilibrium Fe isotope fractionation between aqueous Fe(III) and hematite. *Geochimica et Cosmochimica Acta* **66**, 2995–3015.
Staubwasser M, von Blanckenburg F, Schoenberg R (2006) Iron isotopes in the early marine diagenetic iron cycle. *Geology* **34**, 629–632.
Steinhoefel G, Horn I, von Blanckenburg F (2009) Micro-scale tracing of Fe and Si isotope signatures in banded iron formation using femtosecond laser ablation. *Geochimica et Cosmochimica Acta* **73**, 5343–5360.
Teutsch N, Schmid M, Müller B, Halliday AN, Bürgmann H, Wehrli B (2009) Large iron isotope fractionation at the oxic–anoxic boundary in Lake Nyos. *Earth and Planetary Science Letters* **285**, 52–60.
Thamdrup B (2000) Bacterial manganese and iron reduction in aquatic sediments. *Advances in Microbial Ecology* **16**, 41–84.
Valaas-Hyslop E, Valley JW, Johnson CM, Beard BL (2008) The effects of metamorphism on O and Fe isotope compositions in the Biwabik iron-formation, northern Minnesota. *Contributions to Mineralogy and Petrology* **155**, 313–328.
Vargas M, Kashefi K, Blunt-Harris EL, Lovley DR (1998) Microbiological evidence for Fe(III) reduction on early Earth. *Nature* **395**, 65–67.
Walker JCG (1984) Suboxic diagenesis in banded iron formations. *Nature* **309**, 340–342.
Walker JCG (1987) Was the archaean biosphere upside down? *Nature* **329**, 710–712.
Welch SA, Beard BL, Johnson CM, Braterman PS (2003) Kinetic and equilibrium Fe isotope fractionation between aqueous Fe(II) and Fe(III). *Geochimica et Cosmochimica Acta* **67**, 4231–4250.
Whitehouse MJ, Fedo CM (2007) Microscale heterogeneity of Fe isotopes in >3.71 Ga banded iron formation from the Isua Greenstone Belt, southwest Greenland. *Geology* **35**, 719–722.
Wiederhold JG, Kraemer SM, Teutsch N, Borer PM, Halliday AN, Kretzschmar R (2006) Iron isotope fractionation during proton-promoted, ligand-controlled, and reductive dissolution of goethite. *Environmental Science and Technology* **40**, 3787–3793.
Wu L, Beard BL, Roden EE, Johnson CM (2009) Influence of pH and dissolved Si on Fe isotope fractionation during dissimilatory microbial reduction of hematite. *Geochimica et Cosmochimica Acta* **73**, 5584–5599.
Yamaguchi KE, Johnson CM, Beard BL, Ohmoto H (2005) Biogeochemical cycling of iron in the Archean-Paleoproterozoic Earth: constraints from iron isotope variations in sedimentary rocks from the Kaapvaal and Pilbara Cratons. *Chemical Geology* **218**, 135–169.
Zhabina NN, Volkov II (1978) A method for determination of various sulfur compounds in sea sediment and rocks. In *Environmental Biogeochemistry* (ed. Krumbein WE). Ann Arbor Science Publishers, Ann Arbor, pp. 735–746.

SUPPORTING INFORMATION

Additional Supporting Information may be found in the online version of this article:

Fig. S1 (A) Location of study site located in Shasta County, northern California. (B) Tributaries carry acid mine drainage (AMD) from Iron Mountain to the Spring Creek Reservoir.

Fig. S2 Percent of total citrate/dithionite (CD)-extractable Fe soluble in 0.5 M HCl (1.5 g of pore fluid-free sediment in 10 mL) over time.

Fig. S3 X-ray diffraction (XRD) analyses of anaerobically dried SCAKR sediment, showing the dominant mineralogy as quartz, kaolinite, and the Fe(III) oxides goethite and ferrihydrite.

Fig. S4 Transmission electron microscopic (TEM) images and selected area electron diffraction (SAED) patterns of anaerobically dried SCAKR sediment showing the presence of goethite (A, B) and ferrihydrite (C, D) form aggregates of nanometer-scale grains. These aggregates were generally associated with clay minerals [smectite (S), kaolinite (K) and halloysite] or feldspar (E, F).

Table S1 Summary of geochemical measurements from SCAKR sediment cores and the sediment incubation experiments.

Table S2 Summary of Fe isotope measurements from SCAKR sediment cores and the sediment incubation experiment.

Table S3 Abundance of culturable DIRM at ~150 cm depth in SCAKR core 06GTIM-B.

Table S4 Phylogenetic assignments for 16S rRNA gene sequences (64 total) from the SCAKR sediment clone library.

Supporting Information

Microbial production of isotopically light iron(II) in a modern chemically precipitated sediment and implications for isotopic variations in ancient rocks

George E. Tangalos, Brian L. Beard, Clark M. Johnson, Charles N. Alpers, Evgenya S. Shelobolina, Huifang Xu, Hiromi Konishi & Eric E. Roden

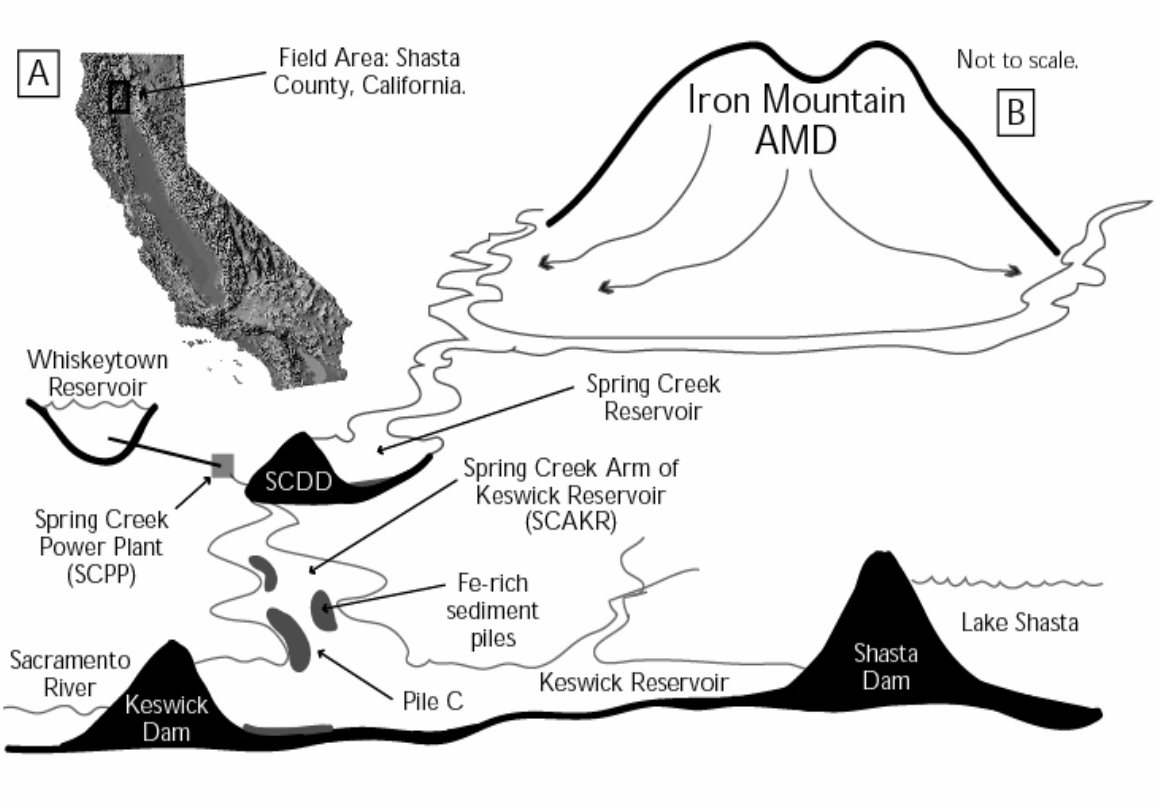

Fig. S1. (A) Location of study site located in Shasta County, northern California. (B) tributaries carry acid mine drainage (AMD) from Iron Mountain to the Spring Creek Reservoir. Historic AMD remediation used controlled AMD releases into the Spring Creek Arm of Keswick Reservoir (SCAKR) through the Spring Creek Debris Dam (SCDD). The AMD mixed with freshwater from the Whiskeytown Reservoir entering via the Spring Creek Power Plant (SCPP), and resulted in the chemical-precipitation of metal-rich sediment in the SCAKR. Modified from Fig. 1 in Nordstrom and Alpers(Nordstrom and Alpers, 1999).

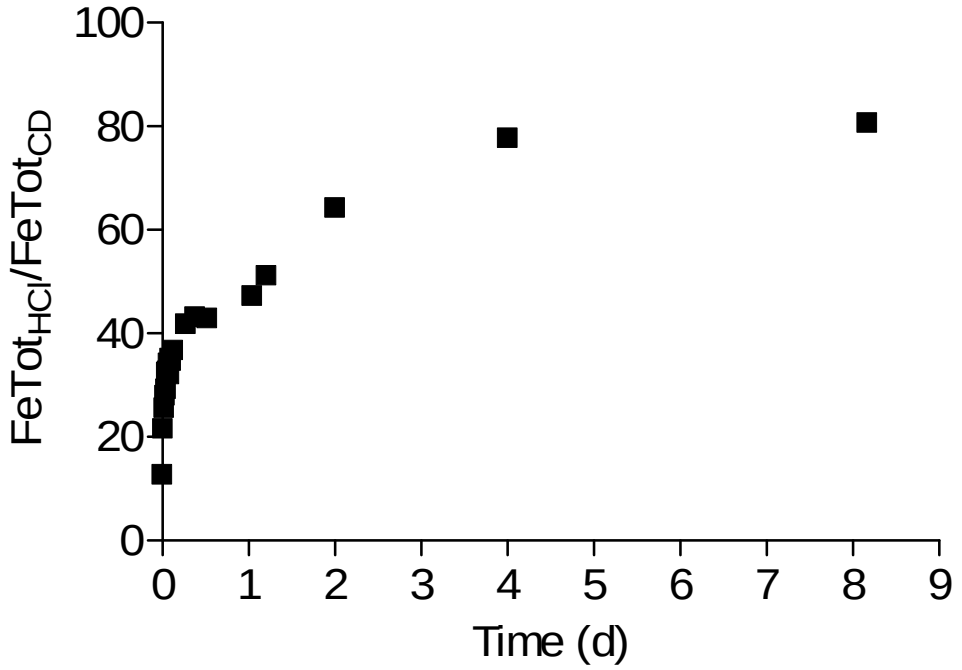

Fig. S2. Percent of total citrate/dithionite (CD)-extractable Fe soluble in 0.5M HCl (1.5 g of pore fluid-free sediment in 10 mL) over time. The initial amount of Fe solubilized in 0.5M HCl approximates the Fe(II) content of the sediment (~13 % of total Fe). After 8 days, ~ 80% of the total CD-extractable Fe was solubilized, which corresponds to dissolution of ~ 75% of the total Fe(III) oxide pool.

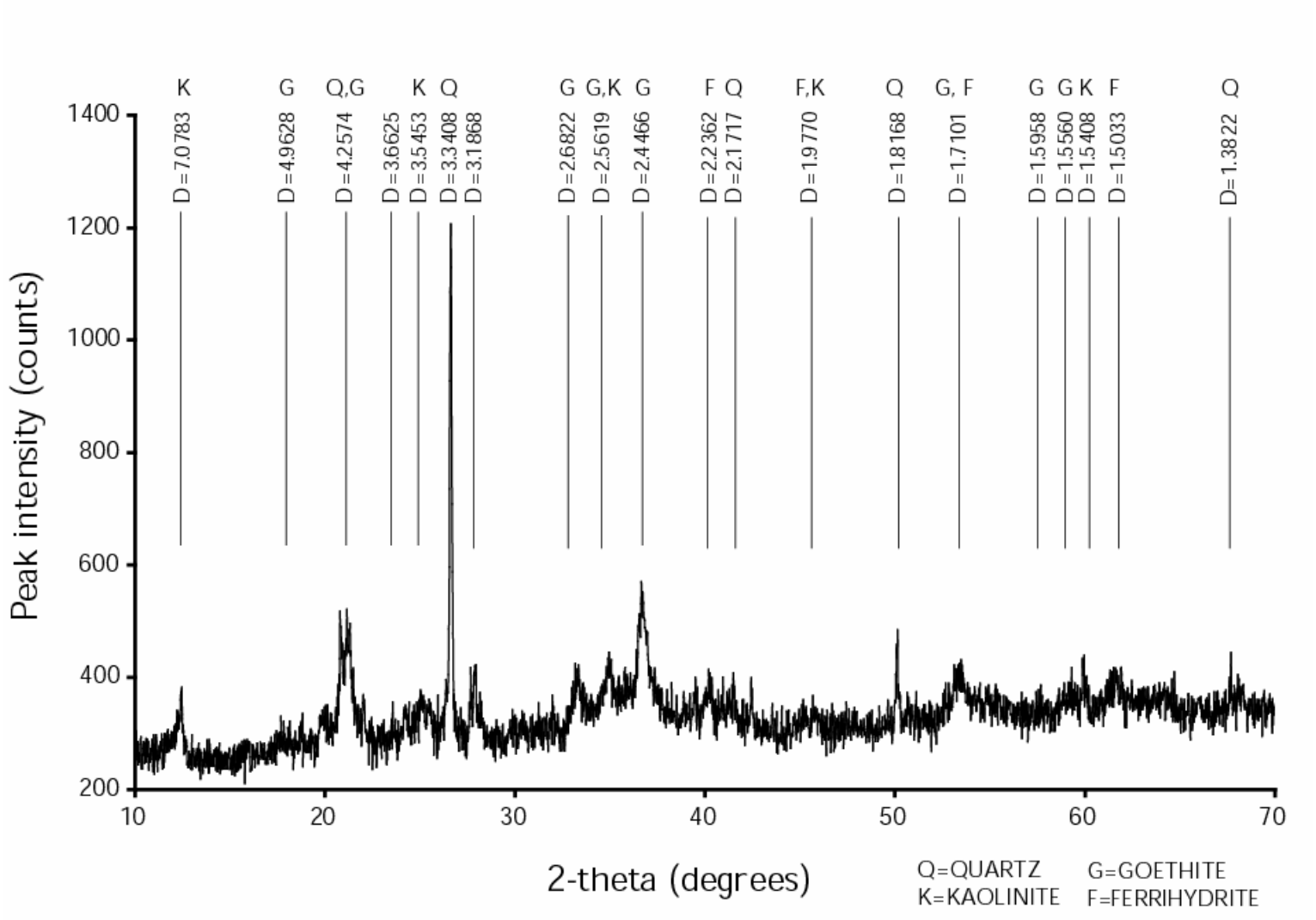

Fig. S3. X-ray diffraction (XRD) analyses of anaerobically-dried SCAKR sediment, showing the dominant mineralogy as quartz, kaolinite, and the Fe(III) oxides goethite and ferrihydrite. The broad peaks and the high background intensity are indicative of poorly-crystalline, nanometer-sized Fe(III) oxide minerals. There was no evidence for the presence of crystalline Fe(II)-bearing phases such as magnetite or siderite. Powdered sediment samples were mounted on a low background quartz sample holder and scanned with a step size of 0.02° and a time interval of 2 seconds.

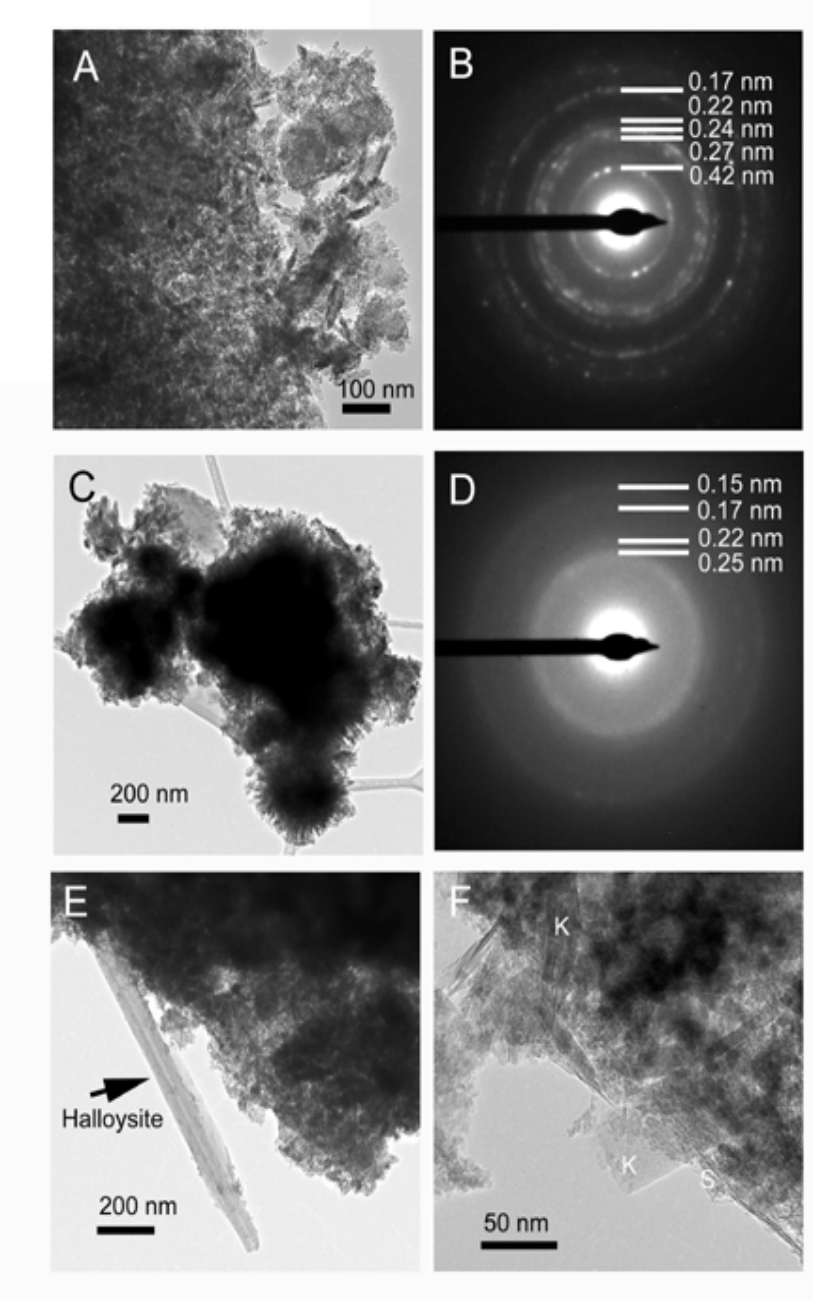

Fig. S4. Transmission electron microscopic (TEM) images and selected area electron diffraction (SAED) patterns of anaerobically-dried SCAKR sediment showing the presence of goethite (A, B) and ferrihydrite (C, D) form aggregates of nanometer-scale grains. These aggregates were generally associated with clay minerals (smectite (S), kaolinite (K) and halloysite) or feldspar (D, E). Extensive examination failed to identify the presence of magnetite or siderite. TEM and SAED measurements were obtained with a Philips CM 200UT microscope (a spherical aberration coefficient (Cs) of 0.5 mm and a point-to-point resolution of 0.19 nm) equipped with an energy-dispersive x-ray spectroscopy (EDX) analyzer (NORAN Voyager), operated at 200 kV.

Table S1[a]. Summary of geochemical measurements from SCAKR sediment cores and sediment incubation experiments. Each data point represents the results of a single analysis on subsamples (~ 1 mL pore fluid or ~ 1 g of pore fluid-free sediment) obtained from 10-20 cm^3 of homogenized material from each sediment core depth interval or sediment incubation experiment.

Sample ID	Depth (cm)	Porosity	pH	Sulfate (mM)	$Fe(II)_{aq}$ (mM)	[b]$Fe(II)_{HCl}$ μmol/g	$FeTot_{HCl}$ μmol/g	$Fe(III)_{HCl}$ μmol/g	$Fe(II)_{HCl}/FeTot_{HCl}$	[c]$FeTot_{CD}$ μmol/g	[d]$Fe(III)_{CD}$ μmol/g	$Fe(III)_{CD}/Fe(III)_{HCl}$	[e]RIS μmol/g	[f]C_{org} wt%
Core 06GTIM-A	30	0.96	6.9	0.0	2.9	760	1770	1009	0.43	2529	1768	1.75	8.9	2.9
	60	0.92	6.6	3.7	7.2	388	893	505	0.43	1451	1063	2.10	5.5	1.5
	90	0.93	6.6	4.3	8.8	664	1449	785	0.46	2167	1503	1.91	26.5	2.9
	120	0.95	6.4	7.4	11.0	1054	3049	1996	0.35	4254	3201	1.60	22.5	3.9
	150	0.87	6.5	7.6	10.7	706	1058	352	0.67	1491	785	2.23	21.3	2.3
	180	0.85	6.4	14.4	13.6	686	1047	361	0.66	1379	692	1.92	52.8	1.8
Core 06GTIM-B	30	0.93	6.7	6.8	3.7	405	636	232	0.64	3065	2660	11.48	[g]-	-
	60	0.95	6.7	9.5	7.5	422	704	282	0.60	2284	1862	6.61	-	-
	90	0.93	6.7	14.0	8.5	482	799	316	0.60	2133	1650	5.21	-	-
	120	0.84	6.6	13.0	10.2	395	468	74	0.84	1178	783	10.64	-	-
	150	0.96	6.6	23.0	10.5	681	1031	350	0.66	2443	1762	5.04	-	-
Core 04CAIM-3	30	0.95	6.6	0.0	3.3	618	687	69	0.90	1196	579	8.34	-	-
	60	0.96	6.4	3.9	5.9	278	408	130	0.68	800	522	4.02	-	-
	90	0.98	6.4	5.5	5.4	220	436	216	0.50	1368	1148	5.31	-	-
	120	0.94	6.3	8.8	6.4	887	1063	176	0.83	2142	1256	7.13	-	-
	150	0.94	6.2	9.5	6.8	792	1247	455	0.64	2514	1722	3.79	-	-
	180	0.98	6.2	8.2	7.9	1060	2052	992	0.52	3323	2263	2.28	-	-
	210	0.95	6.2	14.7	9.2	511	664	153	0.77	891	380	2.48	-	-
	240	0.94	6.2	16.5	9.5	695	1093	398	0.64	2108	1413	3.55	-	-
	270	0.93	6.3	16.0	9.4	301	456	155	0.66	2842	2541	16.37	-	-
	300	0.92	6.4	10.9	6.4	758	845	87	0.90	1282	523	6.02	-	-

Table S1, continued.

Sample ID	Time (d)	Porosity	pH	Sulfate (mM)	$Fe(II)_{aq}$ (mM)	$Fe(II)_{HCl}$ μmol/g	$FeTot_{HCl}$ μmol/g	$Fe(III)_{HCl}$ μmol/g	$Fe(II)_{HCl}/FeTot_{HCl}$	$FeTot_{CD}$ μmol/g	$Fe(III)_{CD}$ μmol/g	$Fe(III)_{CD}/Fe(III)_{HCl}$	RIS μmol/g	C_{org} wt%
Sed Incub #1	0	0.989	-	-	0.1	235	759	525	0.31	-	-	-	-	-
	7	0.989	-	-	1.3	382	1339	957	0.29	-	-	-	-	-
	14	0.989	-	-	3.2	693	1799	1106	0.39	-	-	-	-	-
	23	0.989	-	-	2.3	795	1578	784	0.50	-	-	-	-	-
	60	0.989	-	-	1.4	782	1212	430	0.64	-	-	-	-	-
Sed Incub #2	0	0.989	-	-	0.1	321	1357	1036	0.24	-	-	-	-	-
	7	0.989	-	-	1.2	435	923	488	0.47	-	-	-	-	-
	14	0.989	-	-	3.7	670	1043	373	0.64	-	-	-	-	-
	23	0.989	-	-	2.1	764	1296	533	0.59	-	-	-	-	-
	60	0.989	-	-	1.7	540	884	344	0.61	-	-	-	-	-

[a] Regarding the data shown in Fig. 2: Data shown in panels A and B are averages from core 04CAIM-3 collected in 2004 and cores 06GTIM-A and 06GTIM-B collected in 2006, with the exception of RIS which was analyzed on core 06GTIM-A only. Data in panel C are averages of cores 06GTIM-A and 06GTIM-B. Data in panels D and E are for core 06GTIM-A. Although trends were similar for different cores, there was significant core-to-core variability, and error bars are therefore omitted for the sake of clarity.

[b] Subscript "HCl" refers to 0.5M HCl-extractable Fe.

[c] Subscript "CD" refers to total citrate/dithionite-extractable Fe (0.2M sodium citrate/0.35M acetic acid, pH 4.8, plus 50 mg/mL sodium dithionite), which includes amorphous and crystalline Fe(II) oxides as well as solid-associated Fe(II) (Canfield, 1989).

[d] Computed as $FeTot_{CD} - Fe(II)_{HCl}$.

[e] Reduced inorganic sulfur, determined by Cr(II) extraction.

[f] Organic carbon, determined by X-ray fluorescence.

[g] no measurement.

Table S2. Summary of Fe isotope measurements from SCAKR sediment cores and the sediment incubation experiment. Each data point represents the results of one or two analyses on subsamples (ca. 1 mL pore fluid or ca. 1 g of pore fluid-free sediment) obtained from 10-20 cm^3 of bulk homogenized material from each sediment core depth interval or sediment incubation experiment. Iron isotope analyses followed the methods reported by Beard *et al.* (2003); Fe isotope analyses were performed on 600 ppb Fe solutions that allowed an average external 2-standard deviation precision of ± 0.08 ‰ in $^{56}Fe/^{54}Fe$ and ± 0.11 ‰ in $^{57}Fe/^{54}Fe$ on the 45 replicated analyses. The $\delta^{56}Fe$ and $\delta^{57}Fe$ of the Fe standard (IRMM-014) used to calibrate the instrument during the course of this study were -0.09 ± 0.07 ‰ and -0.13 ±0.10 ‰ (errors 2-SD of the mean; n=58), respectively.

					$Fe(II)_{HCl}$	$FeTot_{HCl}$		Individual analyses				Grand mean[c]	
Sample ID	Extraction Procedure	Sample	Depth (cm)	Aliquot[a]	μmol/g	μmol/g	$Fe(II)_{HCl}/FeTot_{HCl}$	$\delta^{56}Fe$	2-SE[b]	$\delta^{57}Fe$	2-SE	$\delta^{56}Fe$	1-SD
Core 06GTIM-A	Partial sequential	Fe(II)aq	30	1	21.0	21.0	1.00	-0.81	0.02	-1.14	0.02	-0.81	0.02
		Fe(II)aq	60	1	19.7	19.7	1.00	-0.59	0.02	-0.85	0.02	-0.59	0.02
		Fe(II)aq	90	1	31.6	31.0	1.02	-0.61	0.03	-0.89	0.02	-0.61	0.03
		Fe(II)aq	120	1	54.4	54.4	1.00	-1.08	0.02	-1.61	0.02	-1.10	0.03
				1				-1.12	0.02	-1.59	0.02		
		Fe(II)aq	150	1	17.5	17.4	1.01	-0.86	0.03	-1.20	0.03	-0.86	0.03
		Fe(II)aq	180	1	18.2	18.2	1.00	-0.21	0.03	-0.27	0.02	-0.23	0.03
				1				-0.26	0.02	-0.35	0.01		
Core 06GTIM-A	Partial sequential	0.1M HCl-Ext	30	1	353	366	0.97	-0.26	0.02	-0.38	0.02	-0.26	0.02
		0.1M HCl-Ext	60	1	595	661	0.90	0.01	0.02	0.03	0.02	0.01	0.02
		0.1M HCl-Ext	90	1	808	904	0.89	-0.02	0.02	0.03	0.02	-0.02	0.02
		0.1M HCl-Ext	120	1	842	964	0.87	-0.13	0.03	-0.22	0.02	-0.17	0.05
				1				-0.20	0.02	-0.27	0.02		
		0.1M HCl-Ext	150	1	638	653	0.98	-0.47	0.03	-0.65	0.02	-0.47	0.03
		0.1M HCl-Ext	180	1	669	669	1.00	-0.43	0.03	-0.64	0.02	-0.46	0.03
				1				-0.48	0.02	-0.60	0.02		
Core 06GTIM-A	Partial sequential	0.5M HCl-Ext	30	1	88.9	544	0.16	0.46	0.03	0.69	0.02	0.46	0.03
		0.5M HCl-Ext	60	1	65.0	360	0.18	0.56	0.02	0.81	0.02	0.56	0.02
		0.5M HCl-Ext	90	1	86.8	565	0.15	0.39	0.02	0.57	0.02	0.39	0.02
		0.5M HCl-Ext	120	1	86.8	685	0.13	0.15	0.02	0.21	0.02	0.14	0.01
				1				0.13	0.02	0.20	0.02		
		0.5M HCl-Ext	150	1	72.1	459	0.16	0.52	0.03	0.80	0.02	0.52	0.03
		0.5M HCl-Ext	180	1	83.5	357	0.23	0.39	0.03	0.61	0.02	0.39	0.03

Table S2, continued.

Sample ID	Extraction Procedure	Sample	Depth (cm)	Aliquot[a]	$Fe(II)_{HCl}$ μmol/g	$FeTot_{HCl}$ μmol/g	$Fe(II)_{HCl}/FeTot_{HCl}$	Individual analyses $\delta^{56}Fe$	2-SE[b]	$\delta^{57}Fe$	2-SE	Grand mean[c] $\delta^{56}Fe$	1-SD
Core 06GTIM-A	Complete sequential	Fe(II)aq	30	1	21.0	21.0	1.00	-0.81	0.02	-1.14	0.02	-0.81	0.02
		Fe(II)aq	60	1	19.7	19.7	1.00	-0.59	0.02	-0.85	0.02	-0.59	0.02
		Fe(II)aq	90	1	31.6	31.0	1.00	-0.61	0.03	-0.89	0.02	-0.61	0.03
		Fe(II)aq	120	1	54.4	54.4	1.00	-1.08	0.02	-1.61	0.02	-1.10	0.03
				1				-1.12	0.02	-1.59	0.02		
		Fe(II)aq	150	1	17.5	17.4	1.00	-0.86	0.03	-1.20	0.03	-0.86	0.03
		Fe(II)aq	180	1	18.2	18.2	1.00	-0.21	0.03	-0.27	0.02	-0.23	0.03
				1				-0.26	0.02	-0.35	0.01		
Core 06GTIM-A	Complete sequential	0.5M HCl-Ext	30	1	1243	2998	0.41	0.25	0.02	0.37	0.02	0.25	0.02
		0.5M HCl-Ext	60	1	980	1947	0.50	0.30	0.02	0.47	0.02	0.30	0.02
		0.5M HCl-Ext	90	1	1861	3895	0.48	0.14	0.02	0.25	0.02	0.14	0.02
		0.5M HCl-Ext	120	1	2009	4649	0.43	-0.18	0.02	-0.28	0.02	-0.18	0.02
		0.5M HCl-Ext	150	1	1156	2434	0.48	0.09	0.02	0.17	0.02	0.09	0.02
		0.5M HCl-Ext	180	1	717	1379	0.52	0.10	0.02	0.17	0.02	0.09	0.01
				1				0.08	0.02	0.14	0.02		
Core 06GTIM-A	Complete sequential	7M HCl-Ext	30	1	n/a	1315	n/a	-0.15	0.02	-0.19	0.02	-0.15	0.02
		7M HCl-Ext	60	1	n/a	1659	n/a	-0.07	0.03	-0.07	0.02	-0.07	0.03
		7M HCl-Ext	90	1	n/a	2071	n/a	-0.06	0.03	-0.09	0.02	-0.06	0.03
		7M HCl-Ext	120	1	n/a	2642	n/a	-0.26	0.02	-0.34	0.02	-0.26	0.00
				1				-0.3	0.02	-0.37	0.02		
		7M HCl-Ext	150	1	n/a	1109	n/a	-0.06	0.02	-0.10	0.02	-0.06	0.02
		7M HCl-Ext	180	1	n/a	1051	n/a	-0.12	0.02	-0.07	0.03	-0.14	0.02
				1				-0.16	0.01	-0.21	0.01		
Core 06GTIM-A	Complete sequential	29M HF-Ext	30	1	n/a	77.0	n/a	0.15	0.02	0.21	0.02	0.15	0.02
		29M HF-Ext	60	1	n/a	124	n/a	0.18	0.02	0.27	0.02	0.18	0.02
		29M HF-Ext	90	1	n/a	72	n/a	0.10	0.02	0.17	0.01	0.10	0.02
		29M HF-Ext	120	1	n/a	102	n/a	-0.06	0.03	-0.06	0.01	-0.06	0.03
		29M HF-Ext	150	1	n/a	149	n/a	0.03	0.02	0.05	0.02	0.03	0.02
		29M HF-Ext	180	1	n/a	129	n/a	0.06	0.03	0.04	0.02	0.06	0.01

Table S2, continued.

					$Fe(II)_{HCl}$	$FeTot_{HCl}$		Individual analyses				Grand mean[c]	
Sample ID	Extraction Procedure	Sample	Depth (cm)	Aliquot[a]	μmol/g	μmol/g	$Fe(II)_{HCl}/FeTot_{HCl}$	$\delta^{56}Fe$	2-SE[b]	$\delta^{57}Fe$	2-SE	$\delta^{56}Fe$	1-SD
Core 06GTIM-A	Total Digest	29M HF-Ext	30	1	n/a	1168	n/a	0.18	0.02	0.33	0.02	0.18	0.02
		29M HF-Ext	60	1	n/a	1853	n/a	0.09	0.01	0.15	0.01	0.09	0.01
		29M HF-Ext	90	1	n/a	2102	n/a	0.04	0.02	0.09	0.02	0.04	0.02
		29M HF-Ext	120	1	n/a	5233	n/a	-0.29	0.03	-0.44	0.02	-0.29	0.03
		29M HF-Ext	150	1	n/a	1595	n/a	0.08	0.02	0.12	0.01	0.08	0.02
		29M HF-Ext	180	1	n/a	1490	n/a	-0.05	0.02	-0.08	0.02	-0.05	0.02
Core 06GTIM-B	Complete sequential	Fe(II)aq	30	1	33.3	33.3	1.00	-1.48	0.04	-2.15	0.02	-1.46	0.02
				1				-1.45	0.04	-2.17	0.02		
		Fe(II)aq	60	1	39.8	42.0	0.95	-1.55	0.03	-2.22	0.03	-1.54	0.01
				1				-1.53	0.03	-2.24	0.02		
		Fe(II)aq	90	1	34.9	37.3	0.93	-1.00	0.04	-1.47	0.02	-1.04	0.06
				1				-1.08	0.06	-1.67	0.03		
		Fe(II)aq	120	1	14.4	15.5	0.45	-0.47	0.03	-0.72	0.01	-0.50	0.03
				1				-0.53	0.03	-0.73	0.02		
				2	14.4	15.5	0.18	-0.49	0.02	-0.73	0.02		
		Fe(II)aq	150	1	53.4	55.7	0.96	-0.72	0.06	-1.10	0.03	-0.78	0.08
				1				-0.83	0.06	-1.25	0.04		
Core 06GTIM-B	Complete sequential	0.5M HCl-Ext	30	1	210	588	0.36	0.24	0.02	0.40	0.02	0.20	0.05
				2	205	635	0.32	0.17	0.03	0.25	0.02		
		0.5M HCl-Ext	60	1	194	555	0.35	0.17	0.03	0.34	0.02	0.20	0.04
				2	198	601	0.33	0.22	0.04	0.38	0.02		
		0.5M HCl-Ext	90	1	305	680	0.45	0.34	0.03	0.52	0.03	0.31	0.07
				1				0.36	0.03	0.55	0.02		
				2	349	719	0.49	0.22	0.02	0.33	0.02		
		0.5M HCl-Ext	120	1	283	519	0.55	[e]-	-	-	-	0.60	0.04
				2	309	605	0.51	0.60	0.04	0.89	0.02		
		0.5M HCl-Ext	150	1	227	483	0.47	0.40	0.03	0.60	0.02	0.34	0.06
				2	280	581	0.48	0.33	0.05	0.50	0.02		
				2				0.29	0.05	0.45	0.02		

Table S2, continued.

Sample ID	Extraction Procedure	Sample	Depth (cm)	Aliquot[a]	$Fe(II)_{HCl}$ μmol/g	$FeTot_{HCl}$ μmol/g	$Fe(II)_{HCl}/FeTot_{HCl}$	Individual analyses $\delta^{56}Fe$	2-SE[b]	$\delta^{57}Fe$	2-SE	Grand mean[c] $\delta^{56}Fe$	1-SD
Core 06GTIM-B	Complete sequential	7M HCl-Ext	30	1	n/a	1612	n/a	-0.16	0.02	-0.23	0.02	-0.17	0.03
				1				-0.17	0.06	-0.23	0.03		
				1				-0.20	0.05	-0.22	0.02		
				2	n/a	1676	n/a	-0.14	0.02	-0.21	0.02		
		7M HCl-Ext	60	1	n/a	1133	n/a	-0.28	0.03	-0.39	0.02	-0.25	0.02
				2	n/a	1034	n/a	-0.25	0.06	-0.40	0.03		
				2				-0.23	0.03	-0.36	0.02		
		7M HCl-Ext	90	1	n/a	1186	n/a	0.08	0.02	0.13	0.02	0.05	0.04
				2	n/a	1334	n/a	0.07	0.07	0.08	0.02		
				2				0.01	0.02	0.06	0.02		
		7M HCl-Ext	120	1	n/a	1067	n/a	0.27	0.05	0.48	0.02	0.29	0.05
				1				0.24	0.02	0.38	0.02		
				1				0.37	0.05	0.61	0.03		
				2	n/a	1201	n/a	0.29	0.03	0.42	0.02		
		7M HCl-Ext	150	1	n/a	1061	n/a	-0.03	0.02	0.01	0.02	-0.05	0.04
				2	n/a	1067	n/a	-0.02	0.05	-0.08	0.02		
				2				-0.09	0.03	-0.13	0.02		
Core 06GTIM-B	Complete sequential	29M HF-Ext	30	1	n/a	41.7	n/a	-0.20	0.03	-0.25	0.02	-0.21	0.02
				2	n/a	102	n/a	-0.23	0.03	-0.34	0.02		
		29M HF-Ext	60	1	n/a	85.1	n/a	-0.58	0.03	-0.89	0.02	-0.54	0.06
				2	n/a	123	n/a	-0.50	0.03	-0.76	0.02		
		29M HF-Ext	90	1	n/a	79.2	n/a	-0.01	0.02	0.01	0.02	0.00	0.03
				2	n/a	117	n/a	0.04	0.03	0.03	0.02		
				2				-0.01	0.03	-0.05	0.02		
		29M HF-Ext	120	1	n/a	148	n/a	-0.06	0.02	-0.05	0.02	-0.06	0.00
				2	n/a	167	n/a	-0.06	0.05	-0.06	0.02		
		29M HF-Ext	150	1	n/a	306	n/a	-0.22	0.04	-0.31	0.02	-0.20	0.04
				2	n/a	258	n/a	-0.17	0.03	-0.24	0.02		

Table S2, continued.

Sample ID	Extraction Procedure	Sample	Depth (cm)	Aliquot[a]	$Fe(II)_{HCl}$ µmol/g	$FeTot_{HCl}$ µmol/g	$Fe(II)_{HCl}/FeTot_{HCl}$	Individual analyses $\delta^{56}Fe$	2-SE[b]	$\delta^{57}Fe$	2-SE	Grand mean[c] $\delta^{56}Fe$	1-SD
Core 06GTIM-B	Total Digest	29M HF-Ext	30	1	n/a	1091	n/a	0.00	0.03	-0.04	0.02	-0.04	0.03
				1				-0.06	0.03	-0.03	0.02		
				2	n/a	1035	n/a	-0.05	0.03	-0.10	0.02		
		29M HF-Ext	60	1	n/a	671	n/a	-0.02	0.02	-0.01	0.02	-0.10	0.07
				1				-0.15	0.03	-0.17	0.02		
				2	n/a	656	n/a	-0.13	0.02	-0.12	0.02		
		29M HF-Ext	90	1	n/a	1136	n/a	-0.03	0.03	0.00	0.02	0.05	0.09
				1				-0.03	0.05	-0.03	0.04		
				2	n/a	951	n/a	0.10	0.02	0.17	0.02		
				2				0.14	0.03	0.22	0.01		
		29M HF-Ext	120	1	n/a	854	n/a	0.23	0.03	0.41	0.02	0.08	0.21
				2	n/a	1143	n/a	-0.07	0.03	-0.13	0.02		
		29M HF-Ext	150	1	n/a	586	n/a	-	-	-	-	0.03	0.02
				2	n/a	609	n/a	0.03	0.02	0.07	0.01		

Table S2, continued.

Sample ID	Extraction Procedure	Sample	Time (d)	Aliquot[a]	Fe(II) (mmol/L)	FeTot (mmol/L)	$Fe(II)_{HCl}/FeTot_{HCl}$	Individual analysis $\delta^{56}Fe$	2-SE[b]	$\delta^{57}Fe$	2-SE	Grand mean[c] $\delta^{56}Fe$	1-SD
Dry starting sed	Total Digest	29M HF-Ext	n/a	1	n/a	n/a	n/a	0.00	0.02	0.00	0.02	0.00	0.01
		29M HF-Ext	n/a	1	n/a	n/a	n/a	-0.01	0.03	0.02	0.02		
Sed Incub Exp #1	Partial sequential	Fe(II)aq	0	1	0.1	0.3	0.40	-1.68	0.02	-2.50	0.01	-1.68	0.02
		Fe(II)aq	7	1	1.3	1.4	0.91	-1.46	0.02	-2.11	0.02	-1.46	0.01
				1				-1.47	0.02	-2.14	0.02		
		Fe(II)aq	14	1	3.2	3.2	1.02	-0.44	0.02	-0.68	0.02	-0.45	0.01
				1				-0.45	0.01	-0.61	0.02		
		Fe(II)aq	23	1	2.3	2.4	0.99	-0.94	0.02	-1.34	0.02	-0.94	0.02
		Fe(II)aq	60	1	1.4	1.4	0.99	-1.06	0.02	-1.50	0.02	-1.06	0.02
		Fe(II)aq	135	1	2.3	2.3	1.02	0.06	0.02	0.07	0.02	0.06	0.02
Sed Incub Exp #1	Partial sequential	0.1M HCl-Ext	0	1	1.2	2.2	0.55	-0.13	0.02	-0.18	0.02	-0.12	0.01
				1				-0.11	0.02	-0.13	0.02		
		0.1M HCl-Ext	7	1	3.9	4.1	0.94	-0.63	0.02	-0.91	0.02	-0.63	0.02
		0.1M HCl-Ext	14	1	14.5	14.7	0.98	-0.14	0.02	-0.21	0.02	-0.11	0.03
				1				-0.09	0.02	-0.13	0.02		
		0.1M HCl-Ext	23	1	17.1	18.4	0.93	-0.06	0.02	-0.04	0.02	-0.06	0.02
		0.1M HCl-Ext	60	1	19.1	22.0	0.87	-0.02	0.02	0.03	0.03	-0.02	0.02
		0.1M HCl-Ext	135	1	33.8	33.1	1.02	-0.04	0.02	-0.10	0.02	-0.04	0.02
Sed Incub Exp #1	Partial sequential	0.5M HCl-Ext	0	1	5.8	20.6	0.28	0.10	0.03	0.14	0.02	0.10	0.03
		0.5M HCl-Ext	7	1	7.6	36.1	0.21	0.38	0.02	0.59	0.02	0.37	0.02
				1				0.35	0.01	0.58	0.01		
		0.5M HCl-Ext	14	1	6.3	39.3	0.16	0.47	0.02	0.68	0.01	0.47	0.02
		0.5M HCl-Ext	23	1	6.8	29.0	0.23	0.32	0.02	0.51	0.01	0.32	0.02
		0.5M HCl-Ext	60	1	4.3	14.4	0.30	0.36	0.03	0.58	0.02	0.36	0.03

Table S2, continued.

Sample ID	Extraction Procedure	Sample	Time (d)	Aliquot[a]	Fe(II) (mmol/L)	FeTot (mmol/L)	$Fe(II)_{HCl}/FeTot_{HCl}$	Individual analysis $\delta^{56}Fe$	2-SE[b]	$\delta^{57}Fe$	2-SE	Grand mean[c] $\delta^{56}Fe$	1-SD
Sed Incub Exp #2	Partial sequential	Fe(II)aq	0	1	0.1	0.1	0.74	-2.56	0.02	-3.68	0.01	-2.53	0.05
				1				-2.50	0.02	-3.64	0.01		
		Fe(II)aq	7	1	1.2	1.3	0.88	-1.48	0.04	-2.13	0.02	-1.44	0.06
				1				-1.40	0.02	-2.02	0.01		
		Fe(II)aq	14	1	3.7	3.7	1.02	-0.29	0.02	-0.40	0.01	-0.29	0.02
		Fe(II)aq	23	1	2.1	2.1	0.99	-1.11	0.02	-1.64	0.02	-1.11	0.02
		Fe(II)aq	60	1	1.7	1.7	0.99	-1.17	0.02	-1.67	0.02	-1.17	0.02
Sed Incub Exp #2	Partial sequential	0.1M HCl-Ext	0	1	1.3	2.6	0.52	-0.02	0.03	-0.01	0.02	-0.02	0.00
				1				-0.02	0.02	-0.04	0.02		
		0.1M HCl-Ext	7	1	2.9	3.2	0.91	-0.76	0.02	-1.11	0.02	-0.76	0.02
		0.1M HCl-Ext	14	1	13.3	14.4	0.93	-0.08	0.01	-0.10	0.02	-0.08	0.01
		0.1M HCl-Ext	23	1	17.6	18.8	0.94	-0.09	0.02	-0.09	0.02	-0.09	0.02
		0.1M HCl-Ext	60	1	12.3	14.5	0.85	-0.15	0.02	-0.18	0.01	-0.15	0.02
Sed Incub Exp #2	Partial sequential	0.5M HCl-Ext	0	1	8.3	38.2	0.22	0.16	0.02	0.25	0.02	0.16	0.02
		0.5M HCl-Ext	7	1	10.2	24.5	0.41	0.38	0.01	0.55	0.01	0.38	0.01
		0.5M HCl-Ext	14	1	6.8	16.9	0.40	0.45	0.02	0.71	0.02	0.41	0.06
				1				0.37	0.03	0.54	0.02		
		0.5M HCl-Ext	23	1	5.3	20.1	0.26	0.41	0.02	0.61	0.02	0.41	0.02
		0.5M HCl-Ext	60	1	3.9	12.1	0.32	0.25	0.02	0.38	0.02	0.25	0.02

[a] Aliquot number refers to re-processed aliquot from original sample through separate chemical processing.
[b] 2-SE is the internal 2-standard errors based on in-run statistics.
[c] Grand mean is the mean of samples analyzed more than once; 1-SD is one standard deviation of the mean for these samples; for samples that have been analyzed only once, the "in-run" 2-SE is used.
[d] Fe speciation not measured.
[e] isotope sample lost in preparation and not measured.

Table S3. Abundance of culturable DIRB at ~ 150 cm depth in SCAKR core 06GTIM-B. Data represent the mean ± SD of triplicate tubes.

Medium	pH	Electron donor	Cells cm^{-3}
1	6.2	20 mM Acetate	$1.6 \pm 0.3 \times 10^7$
1	6.2	[a] H_2 + 0.5 mM Acetate	$3.0 \pm 2.0 \times 10^6$
2	6.8	20 mM Acetate	$7.5 \pm 1.5 \times 10^6$
2	6.8	H_2 + 0.5 mM Acetate	$6.5 \pm 1.5 \times 10^6$

[a] 100 % (medium 1) or 80 % (medium 2) H_2 gas in the culture tube headspace.

Table S4. Phylogenetic assignments for the 16S rRNA gene sequences (64 total) from the SCAKR sediment clone library. All assignments were made using the National Center for Biotechnology Information (NCBI) Taxonomy Browser. Accession numbers correspond to the closest sequences that could be associated to known Bacterial taxa.

Clone No.	Accession No.	Coverage	Similarity	Phylum	Class	Order	Family	Genus
SCAKR_2	CP000688.1	100%	86%	Chloroflexi	Dehalococcoidetes	Dehalococcoides		Dehalococcoides
SCAKR_3	AY515389.1	96%	97%	Proteobacteria	Betaproteobacteria	Burkholderiales		Paucibacter
SCAKR_4	EU266920.1	99%	90%	Bacteroidetes/Chlorobi				
SCAKR_5	EU266920.1	99%	90%	Bacteroidetes/Chlorobi				
SCAKR_7	AY921931.1	92%	94%	Gemmatimonadetes	Gemmatimonadales			
SCAKR_8	AY515389.1	97%	97%	Proteobacteria	Betaproteobacteria	Burkholderiales		Paucibacter
SCAKR_10	AJ519376.1	86%	99%	Acidobacteria	Acidobacteria	Acidobacteriales	Acidbacteriaceae	Holophaga
SCAKR_11	EF065178.1	96%	99%	Nitrospirae	Nitrospira	Nitrospirales	Nitrospiraceae	Leptospirillum
SCAKR_15	EU266920.1	99%	91%	Bacteroidetes/Chlorobi				
SCAKR_18	CP000655.1	100%	97%	Proteobacteria	Betaproteobacteria	Burkholderiales	Burkholderiaceae	Polynubleobacter
SCAKR_20	U41563.1	93%	97%	Acidobacteria	Acidobacteria	Acidobacteriales	Acidobacteriaceae	Geothrix
SCAKR_21	EF527233.1	100%	97%	Proteobacteria	Deltaproteobacteria	Desulfuromonadales	Geobacteraceae	Geobacter
SCAKR_23	AY879297.1	99%	92%	Proteobacteria	Betaproteobacteria	Rhodocyclales	Rhodocyclaceae	Denitratisoma
SCAKR_24	EU266920.1	99%	90%	Bacteroidetes/Chlorobi				
SCAKR_25	AJ575512.1	99%	99%	Actinobacteria	Actinobacteria			
SCAKR_26	AJ639898.1	100%	97%	Cyanobacteria	Chroococcales			Synechococcus
SCAKR_27	EF133508.1	89%	95%	Proteobacteria	Betaproteobacteria			Ferrovum
SCAKR_29	AY123809.1	98%	92%	Proteobacteria	Betaproteobacteria	Nitrosomonadales	Nitrosomonadaceae	Nitrosospira
SCAKR_30	EU266920.1	99%	91%	Bacteroidetes/Chlorobi				
SCAKR_31	AY515389.1	96%	97%	Proteobacteria	Betaproteobacteria	Burkholderiales		Paucibacter
SCAKR_32	EF016813.1	99%	81%	Actinobacteria	Actinobacteria			
SCAKR_33	EU266843.1	99%	95%	Proteobacteria	Deltaproteobacteria	Syntrophobacterales	Syntrophaceae	
SCAKR_34	EU016422.1	99%	84%	Firmicutes	Clostridia	Clostridiales	Peptococcaceae	
SCAKR_37	AB015525.1	99%	96%	Bacteroidetes	Sphingobacteria	Sphingobacteriales	Flexibacteraceae	Cytophaga
SCAKR_38	AY360547.1	99%	94%	Proteobacteria	Betaproteobacteria	Methylophilales		
SCAKR_41	EU592964.1	99%	89%	Actinobacteria	Actinobacteria	Coriobacteriales	Coroabacteraceae	Olsenella
SCAKR_42	AB072735.1	97%	91%	Gemmatimonadetes	Gemmatimonadetes	Gemmatimonodales	Gemmatimonadaceae	Gemmatimonas
SCAKR_43	AY921931.1	92%	94%	Gemmatimonadetes	Gemmatimonadetes			
SCAKR_44	DQ059300.1	100%	96%	Cyanobacteria				
SCAKR_45	EU266843.1	99%	96%	Proteobacteria	Deltaproteobacteria	Syntrophobacterales	Syntrophaceae	
SCAKR_47	CP000269.1	100%	96%	Proteobacteria	Betaproteobacteria	Burkholderiales	Oxalobacteraceae	Janthinobacterium

Table S4, continued.

Clone No.	Accession No.	Coverage	Similarity	Phylum	Class	Order	Family	Genus
SCAKR_48	AY515389.1	96%	97%	Proteobacteria	Betaproteobacteria	Burkholderiales		Paucibacter
SCAKR_49	CP001016.1	100%	94%	Proteobacteria	Alphaproteobacteria	Rhizobiales	Beijerinckiaceae	Beijerinckia
SCAKR_50	AY515389.1	96%	98%	Proteobacteria	Betaproteobacteria	Burkholderiales		Paucibacter
SCAKR_51	AY921931.1	92%	94%	Gemmatimonadetes	Gemmatimonadales			
SCAKR_52	EU266920.1	99%	90%	Bacteroidetes/Chlorobi				
SCAKR_53	AB072735.1	97%	91%	Gemmatimonadetes	Gemmatimonadetes	Gemmatimonodales	Gemmatimonadaceae	Gemmatimonas
SCAKR_54	DQ383313.1	96%	97%	Proteobacteria	Deltaproteobacteria	Syntrophobacterales	Syntrophaceae	
SCAKR_55	AB109889.1	98%	97%	Proteobacteria	Betaproteobacteria	Burkholderiales	Comamonadaceae	Curvibacter
SCAKR_56	AY515389.1	96%	97%	Proteobacteria	Betaproteobacteria	Burkholderiales		Paucibacter
SCAKR_57	CP000148.1	100%	82%	Proteobacteria	Deltaproteobacteria	Desulfuromonadales	Geobacteraceae	Geobacter
SCAKR_58	AY879297.1	99%	91%	Proteobacteria	Betaproteobacteria	Rhodocyclales	Rhodocyclaceae	Denitratisoma
SCAKR_59	EU266920.1	99%	90%	Bacteroidetes/Chlorobi				
SCAKR_60	AY879297.1	99%	91%	Proteobacteria	Betaproteobacteria	Rhodocyclales	Rhodocyclaceae	Denitratisoma
SCAKR_61	AB109889.1	98%	97%	Proteobacteria	Betaproteobacteria	Burkholderiales	Comamonadaceae	Curvibacter
SCAKR_62	AY918928.1	97%	88%	Bacteroidetes				Prolixibacter
SCAKR_64	AY921932.1	93%	86%	Planctomycete				
SCAKR_67	DQ386262.1	100%	96%	Proteobacteria	Betaproteobacteria	Nitrosomonadales	Gallionellaceae	Gallionella
SCAKR_69	CP000473.1	100%	91%	Acidobacteria	Solibacteres	Solibacterales	Solibacteraceae	Solibacter
SCAKR_71	CP000473.1	100%	92%	Acidobacteria	Solibacteres	Solibacterales	Solibacteraceae	Solibacter
SCAKR_74	EF133508.1	90%	96%	Proteobacteria	Betaproteobacteria			Ferrovum
SCAKR_75	AY918928.1	97%	89%	Bacteroidetes				Prolixibacter
SCAKR_76	AY123809.1	98%	90%	Proteobacteria	Betaproteobacteria	Nitrosomonadales	Nitrosomonadaceae	Nitrosospira
SCAKR_79	AM849456.1	99%	99%	Proteobacteria	Betaproteobacteria			
SCAKR_80	AY691423.1	99%	91%	Proteobacteria	Betaproteobacteria	Rhodocyclales	Rhodocyclaceae	Rhodocyclus
SCAKR_83	EU266843.1	99%	94%	Proteobacteria	Deltaproteobacteria	Syntrophobacterales	Syntrophaceae	
SCAKR_85	AY918928.1	97%	88%	Bacteroidetes				Prolixibacter
SCAKR_87	AB252951.1	98%	85%	Bacteroidetes/Chlorobi				
SCAKR_88	CP000688.1	100%	86%	Chloroflexi	Dehalococcoidetes	Dehalococcoides		Dehalococcoides
SCAKR_91	EU117907.1	100%	97%	Actinobacteria	Actinobacteria			
SCAKR_92	DQ676300.1	95%	93%	Verrucomicrobia				
SCAKR_97	CP000252.1	100%	93%	Proteobacteria	Deltaproteobacteria	Syntrophobacterales	Syntrophaceae	
SCAKR_98	EF520366.1	99%	96%	Actinobacteria	Actinobacteria			
SCAKR_99	AY879297.1	99%	92%	Proteobacteria	Betaproteobacteria	Rhodocyclales	Rhodocyclaceae	Denitratisoma

References

Beard, B. L., C. M. Johnson, J. L. Skulan, K. H. Nealson, L. Cox, and H. Sun. 2003. Application of Fe isotopes to tracing the geochemical and biological cycling of Fe. Chem. Geol. 195:85-117.

Canfield, D. E. 1989. Reactive iron in marine sediments. Geochim. Cosmochim. Acta 53:619-632.

Nordstrom, D. K., and C. N. Alpers. 1999. Negative pH, efflorescent mineralogy, and consequences for environmental restoration at the Iron Mountain Superfund Site, California. Proc. Acad. Nat. Sci. Am. 96:3455-3462.